NMR Quantum Computing

Zhigang Zhang[1], Goong Chen[2], Zijian Diao[3], Philip R. Hemmer[4]

[1] Department of Mathematics, Texas A&M University, College Station, TX 77843 `zgzhang@math.tamu.edu`

[2] Department of Mathematics, Texas A&M University, College Station, TX 77843 `gchen@math.tamu.edu`

[3] Department of Mathematics, Ohio University - Eastern, St. Clairsville, OH 43950 `diao@ohio.edu`

[4] Department of Electrical and Computer Engineering, Texas A&M University, College Station, TX 77843 `prhemmer@ece.tamu.edu`

ABSTRACT

Quantum computing is at the forefront of the scientific and technological research and development of the 21st century. NMR quantum computing is one the most mature technologies for implementing quantum computation. It utilizes the motion of spins of nuclei in custom-designed molecules manipulated by RF pulses. The motion is on a nano- or microscopic scale governed by the Schrödinger equation in quantum mechanics.

In this article, we explain the basic ideas and principles of NMR quantum computing, including basic atomic physics, NMR quantum gates and operations. New progress in optically addressed solid state NMR is expounded. Examples of the Shor's algorithm for factorization of composite integers and quantum lattice-gas algorithm for the diffusion partial differential equation are also illustrated.

1 Nuclear magnetic resonance

Many articles in this book are concerned with mathematical problems in mechanics–elasticity, fluid mechanics, materials, etc., which are of the *macro-scale.* At the other extreme is the study of problems in atoms and molecules, photonics, nanotechnology, etc., which are of the *micro-* or *nano-scale* governed chiefly by the Schrödinger equation. This area has undergone rapid advancements during the past ten years, in large part due to the stimuli from laser applications, quantum computing and quantum technology, and nano-electronics. Most of the practitioners in this area are physicists and it appears that this area has not drawn enough attention from mathematicians. Here,

we wish to describe one of such developments, namely, nuclear magnetic resonance (NMR) quantum computing. There already exist many papers on this topic, see, e.g., [16, 17, 14, 55, 52, 107], written by physicists and computer scientists. Our chapter here describes the same interest, but perhaps from a more mathematical point of view.

1.1 Introduction

As of today, NMR is the most mature technology for the implementation of quantum computing. Naturally, this area is rife with papers. A good internet resource for looking up NMR quantum computing references, both old and new, is the U.S. Los Alamos National Laboratory's web site http://xxx.lanl.gov/quant-ph.

At present, several types of elementary quantum computing devices have been developed, based on AMO (atomic, molecular and optical) or semiconductor physics and technologies. We may roughly classify them into the following:

atomic — ion and atom traps, cavity QED;
molecular — NMR;
semiconductor — coupled quantum dots [11], silicon (Kane) [57];
crystal structure — nitrogen-vacancy (NV) diamond (see Section 3);
superconductivity — SQUID.

The above classification is not totally rigorous as new types of devices, such as quantum dots, or ion traps imbedded in cavity-QED, have emerged which are of the *hybrid* nature. Also, laser pulse control, which is of the optical nature, seems to be omnipresent. In [3], a total of 12 types of quantum computing proposals have been listed[5]. Nevertheless, it is clear that NMR quantum computing belongs to the class of molecular computing where we use molecules as a small computer. The logic bits are the nuclear spins of atoms in custom designed molecules. Spin flips are achieved through the application of radio-frequency (RF) fields on resonance at the nuclear spin frequencies. The system can be initialized by cooling the system down to the ground state or known low-entropy state, or using a special technology called averaging, especially for liquid NMR working in room temperature. Measurement or readout is carried out by measuring the magnetic induction signal generated by the precessing spin on the receiver coil. Numerous experiments have been successfully tried for different algorithms, mostly using liquid NMR technology. The algorithms tested include Grover's search algorithm [106, 52, 44, 120], other generalized search algorithms [73], quantum Fourier transforms [24, 112], Shor's algorithm [109], Deutsch-Jozsa algorithm [13, 71, 25, 82, 22], order finding [105, 98], error correcting code [63], and dense coding [31]. There are

---

[5] The additional proposals not listed above but given in [3] are quantum Hall qubits, electrons in liquid helium, and spin spectroscopies.

also other implementations reported like cat-code benchmark [62], information teleportation [85] and quantum system simulation [96].

NMR is an important tool in chemistry which has been in use for the determination of molecular structure and composition of solids, liquid and gases since the mid 1940s, by research groups in Stanford and MIT independently, led by F. Bloch and E.M. Purcell, both of whom shared the Nobel prize in physics in 1952 for the discovery.

There are many excellent monographs on NMR [29, 89, 79]. There are also many other nice internet website resources offering concise but highly useful information about NMR; cf., e.g., [26, 49, 113]. Let us briefly explain the physics of NMR by following Edwards [26]. The NMR phenomenon is based on the fact that the spin of nuclei of atoms have magnetic properties that can be utilized to yield chemical, physical, and biological information. Through the famous Stern-Gerlach experiment in the earlier development of quantum mechanics, it is known that subatomic particles (protons, neutrons and electrons) have spins. Nuclei with spins behave like a bar magnet in a magnetic field. In some atoms, e.g., ^{12}C(carbon-12), ^{16}O (oxygen-16), ^{32}S(sulphur-32), these spins are paired and cancel each other out so that the nucleus of the atom has no overall spin. However, in many atoms (^{1}H,^{13}C, ^{31}P, ^{15}N, ^{19}F etc.) the nucleus does possess an overall spin. To determine the spin of a given nucleus one can use the following rules:

1. If the number of neutrons and the number of protons are both even, the nucleus has no spin.
2. If the number of neutrons plus the number of protons is odd, then the nucleus has a half-integer spin (i.e., 1/2, 3/2, 5/2).
3. If the number of neutrons and the number of protons are both odd, then the nucleus has an integer spin (i.e., 1, 2, 3).

In quantum mechanical terms, the nuclear magnetic moment of a nucleus can align with an externally applied magnetic field of strength B_0 in only $2I + 1$ ways, either with or against the applied field B_0, where I is the nuclear spin given in (i), (ii) and (iii) above. For example, for a single nucleus with $I = 1/2$, only one transition is possible between the two energy levels. The energetically preferred orientation has the magnetic moment aligned parallel with the applied field (spin $m = +1/2$) and is often denoted as α, whereas the higher energy anti-parallel orientation (spin $m = -1/2$) is denoted as β. See Fig. 1. In NMR quantum computing, these spin-up and spin-down quantum states resemble the two binary states 0 and 1 in a classical computer. Such a nuclear spin can serve as a quantum bit, or *qubit*. The rotational axis of the spinning nucleus cannot be orientated exactly parallel (or anti-parallel) with the direction of the applied field B_0 (aligned along the z axis) but must precess (motion similar to a gyroscope) about this field at an angle, with an angular velocity, ω_0, given by the expression $\omega_0 = \gamma B_0$. The precession rate ω_0 is called the Larmor frequency, cf. Fig. 2. See more discussion of ω_0 below. The constant γ is called the magnetogyric ratio. This precession

process generates an magnetic field with frequency ω_0. If we irradiate the sample with radio waves (MHz), then the proton can absorb the energy and be promoted to the higher energy state. This absorption is called resonance because the frequencies of the applied radiation and the precession coincide at that frequency, leading to resonance.
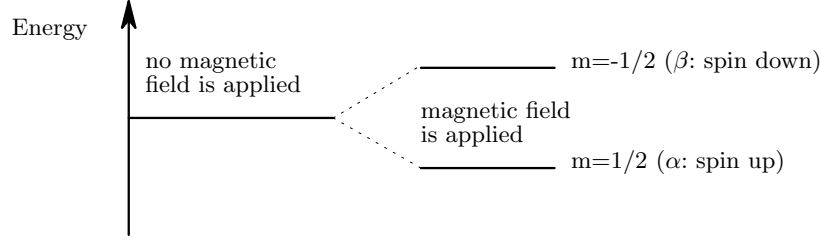
Fig. 1. Splitting of energy levels of a nucleus with spin quantum number 1/2.
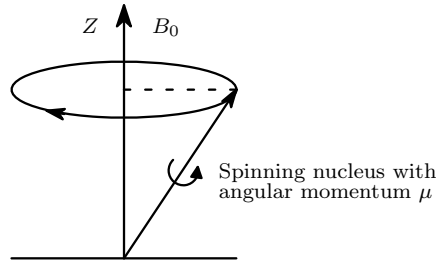
Fig. 2. A magnetic field B_0 is applied along the z-axis, causing the spinning nucleus to precess around the applied magnetic field.

There is another technique related to NMR, called *electron spin resonance (ESR)*, that deals with the spins of electrons instead of those of the nuclei. The principles for ESR are nevertheless similar.

Quantum entanglement is accomplished through spin-spin coupling from the electronic bonds between the nuclei within the molecule and special RF pulse manipulations.

We now examine some fundamentals of the atomic physics that are essential in any quantitative study of the manipulation of the quantum behavior of atoms. A complete description of the Hamiltonian (i.e., energy) of an atom contains 9 terms as follow [29]:

$$H = H_{el} + H_{CF} + H_{LS} + H_{SS} + H_{Ze} + H_{HF} + H_{Zn} + H_{II} + H_Q. \qquad (1)$$

The first three terms have the highest order, called the atomic Hamiltonian. They are the *electronic Hamiltonian term*, *crystal field term*, and the
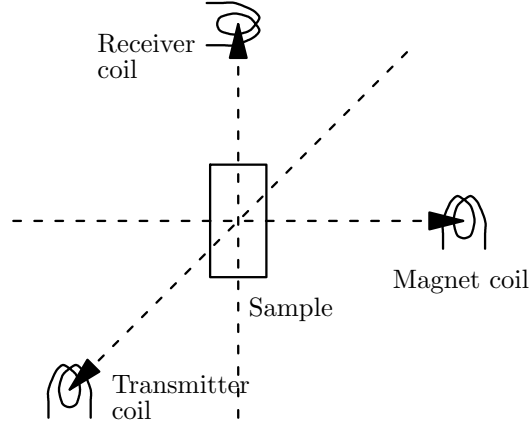
Fig. 3. Schematic of an NMR apparatus. A sample which has non-zero spin nuclei is put in a static magnetic field regulated by the current through the magnet coil. A transmitter coil provides the perpendicular field and a receiver coil picks up the signal. We can change the current through the magnet coil or change the frequency of the current in the transmitter coil to reach resonance.

spin-orbit interaction term, respectively. The electronic Hamiltonian consists of kinetic energy of all electrons, $mv_i^2/2 = p_i^2/2m$, and two Coulomb terms: the potential energy of electrons relative to the nuclei, $-z_n e^2/r_{ni}$, and the inter-electronic repulsion energy, e^2/r_{ij}:

$$H_{el} = \sum_i \frac{p_i^2}{2m} - \sum_{i,n} \frac{z_n e^2}{r_{ni}} + \sum_{i>j} \frac{e^2}{r_{ij}},$$

where r_{ni} denote the distance between the i-th electron with the n-th nucleus, while r_{ij} denote the inter-electronic distance between the i-th and the j-th electrons.

The term H_{CF} is called the crystal field term. It comes from the interaction between the electron and the electronically charged ions forming the crystal, and is essentially a type of electrical potential energy:

$$V = -\sum_{i,j} \frac{Q_j e}{r_{ij}},$$

where Q_j is the ionic charge and r_{ij} is the distance from the electron to the ion. Normally, only those ions nearest to the electron are considered.

The third term in the atomic Hamiltonian is the interaction between spin and orbit:

$$H_{LS} = \lambda \mathbf{L} \cdot \mathbf{S},$$

where $\mathbf{L}$ and $\mathbf{S}$ are the angular momenta of the orbit and spin, respectively, and λ is the coupling constant. In this section, we use $\mathbf{S}$ for the electron spin and $\mathbf{I}$ for the nuclear spin.

The remaining six terms are called *spin Hamiltonians*. Terms H_{Ze} and H_{Zn} are resulted from the application of an external magnetic field:

$$H_{Ze} = \beta \mathbf{B} \cdot (\mathbf{L} + \mathbf{S}),$$

$$H_{Zn} = -\sum_i g_{ni}\beta_n \mathbf{B} \cdot \mathbf{I}_i,$$

where $\mathbf{B}$ is the magnetic field strength. These two terms are called *Zeeman terms*, and they play major roles in NMR and ESR.

The nuclear spin-spin interaction term H_{II} is also important in quantum computation:

$$H_{II} = \sum_{i>j} \mathbf{I}_i \cdot \overleftrightarrow{J}_{ij} \cdot \mathbf{I}_j,$$

because it provides a mechanism for the interaction between qubits. Hyperfine interaction arises from the interaction between the nuclear magnetic moments and the electron:

$$H_{HF} = \mathbf{S} \cdot \sum_i \overleftrightarrow{A}_i \cdot \mathbf{I}_i.$$

In (1), by letting the z-axis be the privileged direction of spin measurement, the spin-spin interaction term H_{SS} is expressed as

$$H_{SS} = D[S_z^2 - \frac{1}{3}S(S+1)] + E(S_x^2 - S_y^2).$$

The very last term in (1) is called the quadrupolar energy:

$$H_Q = \frac{e^2 Q}{4I(2I-1)}\left(\frac{\partial^2 V}{\partial Z^2}\right)(3I_z^2 - I(I+1) + \eta(I_x^2 - I_y^2)).$$

For a specific system, only the Hamiltonian playing major roles is needed in the final model. For example, in the study of ESR, only three terms are retained and the Hamiltonian is written as

$$H = H_{Ze} + H_{HF} + H_{SS},$$

while in the NMR case,

$$H = H_{Zn} + H_{II}.$$

1.2 More about the Hamiltonian of NMR

A classical way to explain NMR is to regard it as a rotating charged particle that acts like a current circulating in a loop ([29, 9]), which creates a magnet with magnetic moment μ, $\mu = qvr/2$, where q is the electronic charge. The particle is rotating at $v/2\pi r$ revolutions per second.

Converting μ to electromagnetic units by dividing it by the velocity of light, and using angular momentum of the particle rather than the velocity of the particle, we obtain

$$\boldsymbol{\mu} = (q/2Mc)\mathbf{p},$$

where $\mathbf{p}$ is the angular momentum oriented along the rotating axis. The ratio μ/p is called the magnetogyric ratio, denoted by γ. A static magnetic field with strength B will apply a torque, which is equal to $\boldsymbol{\mu} \times \mathbf{B}$, on this particle. Newton's law states that the angular momentum will change according to a differential equation

$$\frac{d\mathbf{p}}{dt} = \boldsymbol{\mu} \times \mathbf{B} = \frac{q}{2Mc}\mathbf{p} \times \mathbf{B}.$$

Computation shows that $\mathbf{p}$ will rotate around the direction of $\mathbf{B}$ with frequency ω_0 defined by

$$\omega_0 = \frac{q}{2Mc}B.$$

The above is called the *Larmor equation*, and the frequency ω_0 is called the Larmor frequency, the precession frequency, or the resonance frequency as mentioned previously in Fig. 2.

The above classical considerations are now modified by *quantization* to incorporate the quantum-mechanical behaviors of the nuclear spin. The vector variable $\mathbf{p}$ is quantized with value $\hbar(I(I+1))^{1/2}$, where I is the nuclear spin quantum number, an integer or a half-integer. Its projection to z axis (the direction of the magnetic field) is $m\hbar$. In total, there are $2I + 1$ valid values of m evenly distributed from $-I$ to I, i.e., $m = -I, -I + 1, \cdots, I - 1, I$. A factor g is introduced to include both the spin and orbital motion in the total angular momentum, called the Landé or spectroscopic splitting factor. For a free electron and proton, the magnetic momenta can be given as

$$\mu_e = \frac{g_e}{2}\left(\frac{he}{4\pi M_e c}\right) = \frac{g_e\beta}{2},$$

$$\mu_n = g_n I \left(\frac{he}{4\pi M_N c}\right) = g_n I \beta_N,$$

where $g_e = 2.0023$, $g_n = 5.58490$. Numbers β and β_N are called, respectively, the Bohr and the nucleus magneton where $\beta = 9.27 \times 10^{-21} erg \; gauss^{-1}$ and $\beta_N = 5.09 \times 10^{-24} erg \; gauss^{-1}$. These values vary for different particles. In NMR, it is convenient to use the resonance frequency ω_0:

$$\hbar\omega_0 = g_e\beta B,$$

$$\hbar\omega_0 = g_N I \beta_N B.$$

Now we can write the Hamiltonian of a free nucleus as

$$H = -\boldsymbol{\mu} \cdot \mathbf{B} = -\hbar\gamma\mathbf{I} \cdot \mathbf{B}, \tag{2}$$

where γ is the magnetogyric ratio defined by $\gamma = \frac{\mu}{I\hbar}$ just as in the classical case. It is a characteristic constant for every type of nuclei; different nuclei

have different magnetogyric ratios. Vector **I** after quantization, becomes the operator of angular momentum. The eigenvalues of this system, or the energy levels are

$$E = \gamma \hbar m B, \quad m = -I, -I+1, \cdots, I-1, I. \tag{3}$$

The difference between two neighboring energy levels is $\gamma \hbar B$, which defines the resonance frequency depending on the magnetic field B and the particle.

There are other factors to be considered. The resonance frequency changes with the chemical environment of the nucleus. An example is the fluorine resonance spectrum of perfluorioisopropyl iodide. Two resonance lines of fluorine are observed in the spectrum, and the intensities ratio 6:1 agrees with the population ratio of the two groups of fluorine atoms. This phenomenon, called the *chemical shift*, is proportional to the strength of the magnetic field applied. This effect comes up because electrons close to the nucleus change the magnetic field around it; in other words, they create a diamagnetic shielding surrounding the nucleus. If the static field applied is B_0, then the electrons precessing around the magnetic field direction produce an induced magnetic field opposing B_0. The total effective magnetic field around the nucleus is then

$$\mathbf{B} = \mathbf{B}_0 - \mathbf{B}' = (1 - \sigma)\mathbf{B}_0,$$

where the parameter σ is called *shielding coefficient*. In some cases σ is dependent on the temperature.

High resolution NMR spectroscopy has found that the chemical shifted peaks are also composed of several lines, a result of the spin-spin coupling, which is the second term in the NMR Hamiltonian:

$$H_{II} = \sum_{i>j} \mathbf{I_i} \cdot J_{ij} \cdot \mathbf{I_j}.$$

1.3 Organization of the paper

Section 1 so far has introduced some basic facts of nuclear spins and atomic physics.

In Section 2, we will give a motivation of what quantum computing is about, and introduce universal quantum gates based on liquid NMR.

Section 3 describes the most recent progress in solid state NMR quantum gate controls and designs.

Section 4 and 5 explains applications of the NMR quantum computer to the Shor's algorithm and a lattice gas algorithm.

2 Basic technology used in quantum computation with NMR

2.1 Introduction to quantum computation

Quantum mechanics is one of the revolutionary scientific discoveries of the 20th century. The field of quantum computation, our emphasis in this arti-

cle, was born when the principles of quantum mechanics were introduced to modern computer science. Quantum computation mainly studies the analysis and construction of quantum algorithms with an eye toward surpassing the classical counterparts. Another tightly connected field is quantum information, which deals more with the storage, compression, encryption, and communication of information by quantum mechanical means [38, 6]. Quantum teleportation [5, 10] and quantum cryptography [?, 27] are two of the most known subjects of this field.

Modern computer science emerged when the eminent British mathematician Alan Turing invented the concept of Turing machine (TM) in 1936 [101]. Though very simple and primitive, TM captures the essence of computation. It serves as the universal model for all known physical computation devices. For many years, quantum effects had never been considered in the theory of computation, until the early 1980's. Benioff [4] first coined the term of quantum Turing machine (QTM). Motivated by the problem that classical computers can not simulate quantum systems efficiently, Feynman [33] posed the quantum computer as a solution. Now we know that, in terms of computability, quantum computers and classical computers possess exactly the same computational power. But in terms of computational complexity, which measures the efficiency of computation, there are many exciting examples confirming that quantum computers do solve certain problems faster. The two most significant ones are Shor's factorization algorithm [94] and Grover's search algorithm [44], among other examples such as the Deutsch-Jozsa problem [22], the Bernstein-Vazirani problem [8], and Simon's problem [95].

Current physical realization of quantum computers follows the quantum circuit model [21], instead of the QTM model. Quantum circuit model is another fundamental model of computation, which is equivalent to the QTM model [116], but easier to implement. This model shares many common features of the classical computers. In a classical computer, information is encoded in multi-bits binary states (0 or 1), transferred from one register to another, and processed by logic gates in concatenation. In a quantum computer, information is represented by the quantum states of the qubits, and manipulated by various quantum control mechanisms. Those control mechanisms trigger quantum operation to process information in a way resembling the gates in a classical computer. Such quantum operations are called *quantum gates* and a series of quantum gates in concatenation constitute a *quantum circuit* [110]. However, because of the special effects of quantum mechanics, major distinctions exist.

In contrast to a classical system, a quantum system can exist in different states at the same time, an interesting phenomenon called *superposition*. Superposition enables quantum computers to process data in parallel. That is why a quantum computer can solve certain problems faster than a classical computer. From now on, we will use the Dirac bra-ket notation. In this notation a pure one-qubit quantum state can be written as $|\phi\rangle = a|0\rangle + b|1\rangle$. Here $|0\rangle$ and $|1\rangle$ are the two basis states of the qubit, e.g., in NMR, the spin-up

and spin-down states, and $a, b \in \mathbf{C}$ with $|a|^2 + |b|^2 = 1$. When we make a measurement of a qubit, the result might be either $|0\rangle$ or $|1\rangle$, with probabilities $|a|^2$ and $|b|^2$ respectively. More generally, a string of n qubits can exist in any state of the form $|\psi\rangle = \sum_{x=00\ldots0}^{11\ldots1} \psi_x |x\rangle$, where $\psi_x \in \mathbf{C}$ and $\sum |\psi_x|^2 = 1$. When we make a measurement on $|\psi\rangle$, it collapses to $|x\rangle$, one of the 2^n basis states, with probability $|\psi_x|^2$. This indeterministic nature makes the design of efficient quantum algorithms highly non-trivial.

Another distinctive feature of the quantum circuit is that the operations performed by quantum gates must be unitary ($U^\dagger U = I$). It is the natural consequence of the unobserved quantum systems evolving according to the Schrödinger equation. A quantum gate may operate on any number of qubits. Here are some examples (cf. Fig. 4 for the circuit diagrams):

NOT gate   Hadamard gate   phase gate

CNOT gate   controlled-phase gate
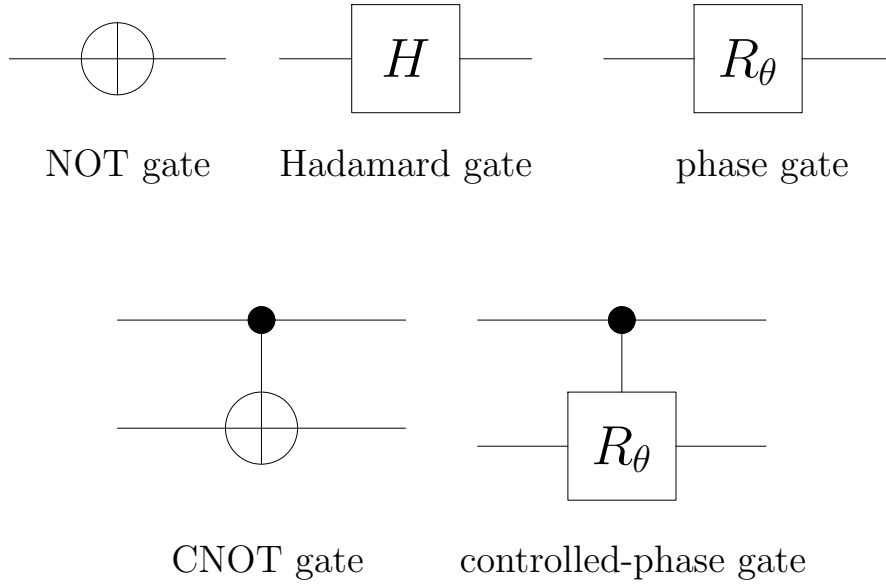
Fig. 4. Circuit diagrams of the NOT/Hadamard/phase/CNOT/controlled-phase gate.

1. NOT gate Λ_0: $\Lambda_0|0\rangle = |1\rangle$, $\Lambda_0|1\rangle = |0\rangle$, or $\Lambda_0 = \begin{bmatrix} 0 & 1 \\ 1 & 0 \end{bmatrix}$.

2. The Hadamard gate H: $H|0\rangle = \frac{1}{\sqrt{2}}(|0\rangle + |1\rangle)$, $H|1\rangle = \frac{1}{\sqrt{2}}(|0\rangle - |1\rangle)$, or

$$H = \frac{1}{\sqrt{2}} \begin{bmatrix} 1 & 1 \\ 1 & -1 \end{bmatrix}.$$

3. One-qubit phase gate R_θ: $R_\theta|0\rangle = |0\rangle$, $R_\theta|1\rangle = e^{i\theta}|1\rangle$, or

$$R_\theta = \begin{bmatrix} 1 & 0 \\ 0 & e^{i\theta} \end{bmatrix}.$$

4. Two-qubit controlled-NOT (CNOT) gate Λ_1: $\Lambda_1|00\rangle = |00\rangle$, $\Lambda_1|01\rangle = |01\rangle$, $\Lambda_1|10\rangle = |11\rangle$, $\Lambda_1|11\rangle = |10\rangle$, or,

$$\Lambda_1 = \begin{bmatrix} 1 & 0 & 0 & 0 \\ 0 & 1 & 0 & 0 \\ 0 & 0 & 0 & 1 \\ 0 & 0 & 1 & 0 \end{bmatrix}.$$

5. Two-bit controlled-phase gate $\Lambda_1(R_\theta)$, where R_θ is the one-bit phase gate: $\Lambda_1(R_\theta)|00\rangle = |00\rangle$, $\Lambda_1(R_\theta)|01\rangle = |01\rangle$, $\Lambda_1(R_\theta)|10\rangle = |10\rangle$, $\Lambda_1(R_\theta)|11\rangle = e^{i\theta}|11\rangle$, or,

$$\Lambda_1(R_\theta) = \begin{bmatrix} 1 & 0 & 0 & 0 \\ 0 & 1 & 0 & 0 \\ 0 & 0 & 1 & 0 \\ 0 & 0 & 0 & e^{i\theta} \end{bmatrix}.$$

The one-qubit and two-qubit quantum gates are of particular importance to the construction of a quantum computer, because of the following universality result.

Theorem 2.1 *(D. DiVincenzo [2, 23]) The collection of all the one-qubit gates and the two-qubit CNOT gate suffice to generate any unitary operations on any number of qubits.*   □

Fig. 5 illustrates, as an example, how to generate the two-qubit controlled-phase gate using 2 CNOT gates and 3 one-qubit phase gates. The controlled-phase gate is an important building block for the quantum Fourier transform; cf. Fig. 14 and Fig. 15.
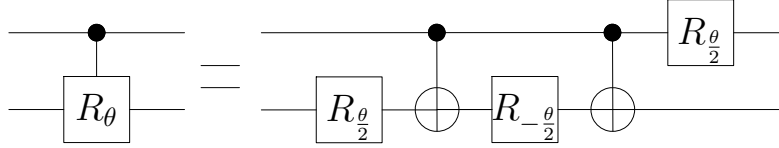
Fig. 5. Construction of the controlled-phase gate with CNOT gates and phase gates.

The standard procedure of executing a quantum algorithm on a quantum circuit usually follows these steps:

1. Initialize the qubits.
2. Apply a proper sequence of quantum gates on the qubits.
3. Measure the qubits.

We will address the details of these steps in the scenario of NMR technology.

2.2 Realization of a qubit

As mentioned in Section 1, NMR quantum computing is accomplished by using the spin-up and spin-down states of a spin-$\frac{1}{2}$ nucleus. A molecule with several nuclear spins may work as a quantum computer where each spin constitutes a *qubit*. In fact, NMR has a long history in information science. Back in the 1950s, nuclear spins were already proposed for information storage in computers.

Liquid NMR receives more interest due to its mature technology and readiness for application. For now, spin-$\frac{1}{2}$ nuclei such as proton and ^{13}C are preferred because they naturally represent a qubit, but multi-level qubits formed by spin-n nuclei, $n = 1, 2, \cdots$, may provide more freedom in the future. Through careful design, the potential qubits or nuclei are configured with different resonance frequencies and can be distinguished from each other. In a low viscosity liquid, dipolar coupling between nuclei is averaged out by the random motion of the molecules. The J-coupling (scalar coupling) dominates the spin-spin interaction, which is an indirect through-bond electronic interaction. Previously, a very difficult part of the system operation was to set the quantum system to a special state (or to initialize it). Now a very complicated technology has been developed to solve this problem.
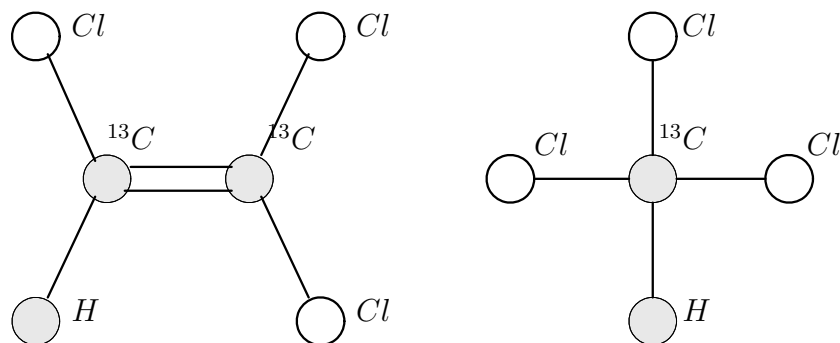
Fig. 6. The molecule structure of a candidate 3-qubit quantum system, trichloroethylene (left), and a candidate 2-qubit quantum system, chloroform. The trichloroethylene molecule has two labelled ^{13}C and a proton, all having one-half-spin nuclei. The chloroform has one labelled ^{13}C and one proton.

Fig. 6 shows the structure of a trichloroethylene (TCE) molecule and a chloroform molecule used in NMR quantum computers. The hydrogen nucleus (proton) and two ^{13}C nuclei in a TCE molecule form three qubits which can be manipulated, while the chloroform molecule provides two qubits. The sample used by an NMR quantum computer has a large number ($\sim 10^{23}$) of such molecules. This is also called a *bulk* quantum computer. Although most molecules are in a totally random state at room temperature, there are still

a small amount of spins standing out and serving our purpose. Theoretically, we use a statistical spin state called a pseudo-pure state, which has the same transformation property as that of a pure quantum state.

Let $|\phi\rangle = a|0\rangle + b|1\rangle$ be the state of a single qubit, $|0\rangle$ for spin-up and $|1\rangle$ for spin-down. We also assume that a is real since only the relative phase is important. Thus this state can be represented using two angles θ and ψ:

$$|\phi\rangle = \cos\frac{\theta}{2}|0\rangle + e^{i\psi}\sin\frac{\theta}{2}|1\rangle, \tag{4}$$

where $\theta \in [0, \pi]$ and $\psi \in [0, 2\pi)$. If we think $|0\rangle$ and $|1\rangle$ as the standard basis in $\mathbf{C}^2$, the quantum state corresponds to a unit vector in $\mathbf{C}^2$.

For the study of NMR spectroscopy with many nuclei, density matrices are preferred and are often written as the linear combination of *product operators* [81]:

$$\begin{aligned}
\rho &= |\phi\rangle\langle\phi| \\
&= \begin{bmatrix} \cos^2\frac{\theta}{2} & e^{-i\psi}\frac{\sin\theta}{2} \\ e^{i\psi}\frac{\sin\theta}{2} & \sin^2\frac{\theta}{2} \end{bmatrix} \\
&= I_0 + \sin\theta\cos\psi I_x + \sin\theta\sin\psi I_y + \cos\theta I_z, \tag{5}
\end{aligned}$$

where the product operators are defined as

$$I_0 = \frac{1}{2}\begin{bmatrix} 1 & 0 \\ 0 & 1 \end{bmatrix}, \quad I_x = \frac{1}{2}\begin{bmatrix} 0 & 1 \\ 1 & 0 \end{bmatrix}, \quad I_y = \frac{1}{2}\begin{bmatrix} 0 & -i \\ i & 0 \end{bmatrix}, \quad I_z = \frac{1}{2}\begin{bmatrix} 1 & 0 \\ 0 & -1 \end{bmatrix}. \tag{6}$$

They are different from the Pauli matrices only by a constant factor and share the similar commutative law. Upon collecting all the coefficients of I_x, I_y, and I_z together, we obtain a vector

$$\mathbf{v} = [\sin\theta\cos\psi \quad \sin\theta\sin\psi \quad \cos\theta]^T,$$

which is called a *Bloch vector*. In essence, we have defined a mapping from the set of unit vectors $|\phi\rangle \in \mathbf{C}^2$ to the set of unit vectors $\mathbf{v} \in \mathbf{R}^3$. We have good reasons to ignore the coefficient of I_0, since it has no effect on the spectroscopy and remains unchanged under any unitary transformation. Each Bloch vector determines a point on the unit sphere, called the *Bloch sphere*, which is displayed in Fig. 7 [80, 81]. Bloch vectors have proven to be a very good tool for NMR quantum operations.

The mapping defined above is surjective, because every point on the Bloch sphere gives rise to a unit vector $\mathbf{v} = [\sin\theta\cos\psi \quad \sin\theta\sin\psi \quad \cos\theta]^T$ for some pair of (θ, ψ). Conversely, if $\mathbf{v}(\theta', \psi') = \mathbf{v}(\theta, \psi)$, we get

$$\begin{cases} \cos\theta &= \cos\theta', \\ \sin\theta\cos\psi = \sin\theta'\cos\psi', \\ \sin\theta\sin\psi = \sin\theta'\cos\psi', \end{cases} \tag{7}$$

which can be used to show that the mapping is also injective if we identify all pairs of $(0, \psi)$ with the north pole and all pairs of (π, ψ) with the south pole. In fact, these two sets correspond to two states $|0\rangle$ and $|1\rangle$, respectively.
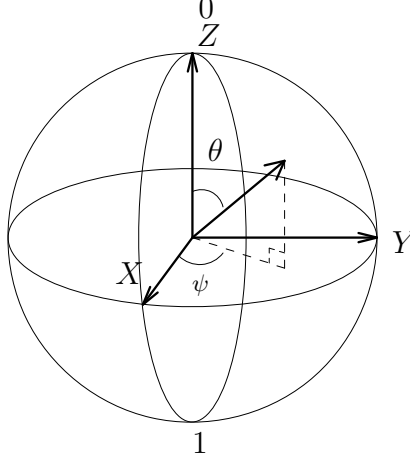
Fig. 7. The Bloch sphere representation of a quantum state.

2.3 Transformation of quantum states: SU(2) and SO(3)

When a quantum operation is applied to a quantum system, it may change the quantum state of the system from one to another. The representation of the operation depends on how the quantum state is represented. For example, (4) leads to an operator or matrix U which connects the new and old states of a single spin quantum system:

$$|\phi'\rangle = U|\phi\rangle,$$

where $|\phi'\rangle$ and $|\phi\rangle$ are the quantum state after and before the operation, respectively. The fact that both states are unit vectors implies that U is a 2×2 unimodular complex matrix. Moreover, U is also unitary, i.e., $U \in \mathbf{SU}(2)^6$, a Lie group endowed with a certain topology.

   If the quantum state is represented by a three-dimensional Bloch vector, the effect of a unitary operation can be viewed as that of a rotation which rotates the Bloch sphere, and the operator is represented by a 3×3 real matrix S. If the quantum system has states $\mathbf{v}$ and $\mathbf{v}'$ in Bloch vector form before and after the operation, respectively, then

---

[6] $\mathbf{SU}(n)$ is the special unitary group of $n \times n$ matrices. An $n \times n$ matrix $A \in \mathbf{SU}(n)$ if and only if A is unitary, i.e., $A \cdot A^\dagger = I_n$, where $A^\dagger$ is the Hermitian adjoint of A, and $\det A = 1$.

$$\mathbf{v}' = S\mathbf{v}.$$

The matrix S is a proper rotation matrix, i.e., $S \in \mathbf{SO}(3)$[7]. It is isometric and preserves the three-fold product.

If both S and U represent the same physical operation, such as a transformation induced by a series of pulses in NMR, there must be a connection between them. One can show that there is a mapping R from $\mathbf{SU}(2)$ to $\mathbf{SO}(3)$ such that $S = R(U)$, for any $U \in \mathbf{SU}(2)$ and its corresponding Bloch-sphere representation S [86]. Simple computation shows that the entry of matrix $S = R(U)$ at the kth row and i^{th} column is given as

$$S_{ki} = Tr(\sigma_k \, U \, I_i \, U^\dagger), \tag{8}$$

where σ_k are the Pauli matrices[8], and Tr is the trace operator. It can also be shown that R is a two-to-one homomorphism between $\mathbf{SU}(2)$ and $\mathbf{SO}(3)$ with kernel $ker(R) = \{I, -I\}$. It coincides with the fact that U and $-U$ in $\mathbf{SU}(2)$ represent the same operation because only the relative phase matters. This mapping is also surjective, so it defines an isomorphism from the quotient group $\mathbf{SU}(2)/ker(R)$ to $\mathbf{SO}(3)$. We provide a more detailed discussion about this isomorphism in the Appendix.

It is known that any $U \in \mathbf{SU}(2)$ can be written into an exponential form parameterized by a angle $\theta \in [0, 2\pi)$ and a unit vector $\mathbf{n}$ such that

$$\begin{aligned} U(\theta, \mathbf{n}) &= e^{-i\frac{\theta}{2}\mathbf{n}\cdot\boldsymbol{\sigma}} \\ &= \begin{bmatrix} \cos\frac{\theta}{2} - in_3\sin\frac{\theta}{2} & -\sin\frac{\theta}{2}(n_2 + in_1) \\ \sin\frac{\theta}{2}(n_2 - in_1) & \cos\frac{\theta}{2} + in_3\sin\frac{\theta}{2} \end{bmatrix} \\ &= \cos\frac{\theta}{2}I - i\sin\frac{\theta}{2}\mathbf{n}\cdot\boldsymbol{\sigma}, \end{aligned} \tag{9}$$

where $\boldsymbol{\sigma} = [\sigma_x, \sigma_y, \sigma_z]$. With this parameterization of $\mathbf{SU}(2)$, entries of $S = R(U)$ can be computed using (8) as

$$S_{ij} = R(U)_{ij} = \cos\theta \, \delta_{ij} + (1 - \cos\theta)n_i n_j + \sum_{k=1}^{3}\sin\theta \, \epsilon_{ikj}n_k. \tag{10}$$

It should be noted now that S coincides with a rotation about the axis along $\mathbf{n}$ with an angle θ in the three dimensional Euclidean space after comparing S_{ij} with the standard formula of a rotation matrix. This interpretation is important in understanding the terminologies used in NMR. For example, the rotations around x, y, and z axes ($x/y/z$-rotations) with an arbitrary angle θ define the following three unitary operators in $\mathbf{SU}(2)$, respectively:

---

[7] $\mathbf{SO}(3)$ denotes the special orthogonal group of 3×3 matrices. An $n \times n$ matrix $A \in \mathbf{SO}(n)$ if and only if A is real, $AA^T = I_n$ and $\det A = 1$.

[8] The Pauli matrices are $\sigma_x = \begin{bmatrix} 0 & 1 \\ 1 & 0 \end{bmatrix}$, $\sigma_y = \begin{bmatrix} 0 & -i \\ i & 0 \end{bmatrix}$, and $\sigma_z = \begin{bmatrix} 1 & 0 \\ 0 & -1 \end{bmatrix}$.

$$X_\theta = e^{-i\theta\sigma_x/2} = \begin{bmatrix} \cos\frac{\theta}{2} & -i\sin\frac{\theta}{2} \\ -i\sin\frac{\theta}{2} & \cos\frac{\theta}{2} \end{bmatrix}, \tag{11}$$

$$Y_\theta = e^{-i\theta\sigma_y/2} = \begin{bmatrix} \cos\frac{\theta}{2} & -\sin\frac{\theta}{2} \\ \sin\frac{\theta}{2} & \cos\frac{\theta}{2} \end{bmatrix}, \tag{12}$$

$$Z_\theta = e^{-i\theta\sigma_z/2} = \begin{bmatrix} e^{-i\theta/2} & 0 \\ 0 & e^{i\theta/2} \end{bmatrix}. \tag{13}$$

2.4 Construction of quantum gates

From Theorem 2.1, we know that the collection of all the one-qubit gates and the two-qubit CNOT gate are universal. In addition, the following fact [83, p. 175] holds for one-qubit quantum gates:

Theorem 2.2 *Suppose U is a unitary operation on a single qubit. Then there exist real numbers α, β, γ, and δ such that*

$$U = e^{i\alpha} Z_\beta Y_\gamma Z_\delta.$$

$$\square$$

For example, the Hadamard gate H can be decomposed as $H = e^{-i\frac{\pi}{2}} Y_{\pi/2} Z_\pi$. Clearly, the $x/y/z$ rotation gates provide building blocks sufficient to construct any one qubit unitary gate. In this subsection, we will show how to realize these one-qubit rotation gates and the two-qubit CNOT gate using NMR. We will also show how to decouple the interaction between two spins, a process called *refocusing* [83].

One-qubit gates

A single spin system has Hamiltonian $H = -\boldsymbol{\mu} \cdot \mathbf{B}$, where $\boldsymbol{\mu}$ is the magnetic moment, and

$$\mathbf{B} = B_0\mathbf{e}_z + B_1(\mathbf{e}_x \cos(\omega t) + \mathbf{e}_y \sin(\omega t)) \tag{14}$$

is the magnetic field applied. B_0, a large constant, is the amplitude of the static magnetic field, and B_1 is the amplitude of the oscillating magnetic field in the x-y plane. When $B_1 = 0$, the Hamiltonian and Schrödinger equation can be obtained as ([83])

$$H = \frac{\omega_0}{2}\sigma_z \tag{15}$$

and

$$i\partial_t|\psi(t)\rangle = H|\psi(t)\rangle, \tag{16}$$

respectively, where $\hbar$ has been divided from both sides in the second equation and we take $\hbar$ away from H in the first one just for simplicity. The Larmor frequency $\omega_0 = -B_0\gamma$ is defined by the nuclei and the magnetic field, see (3). Assume that the initial state is $|\psi_0\rangle = a_0|0\rangle + b_0|1\rangle$. Then the evolution of the

quantum state of the spin and the density matrix can be solved directly and given as

$$|\psi(t)\rangle = e^{-i\omega_0\sigma_z t/2}|\psi_0\rangle$$
$$= \begin{bmatrix} e^{-i\omega_0 t/2} & 0 \\ 0 & e^{i\omega_0 t/2} \end{bmatrix} \begin{bmatrix} a_0 \\ b_0 \end{bmatrix}$$
$$= e^{-i\omega_0 t/2} \begin{bmatrix} 1 & 0 \\ 0 & e^{i\omega_0 t} \end{bmatrix} |\psi_0\rangle,$$
$$\rho(t) = e^{-itH}\rho(0)e^{itH}.$$

This evolution is also called a *chemical shift evolution*, resembling the precessing of a magnet in a static field. Recall the Bloch vector on the Bloch sphere. It is exactly Z_θ, the rotation operator around the z axis with $\theta = \omega_0 t$.

To achieve an x-rotation operator, we need a small magnetic field transverse to the z direction to control the evolution of the quantum state. The Hamiltonian is given as in (14) by choosing B_1 different from zero:

$$H = -\boldsymbol{\mu} \cdot \mathbf{B} = \frac{\omega_0}{2}\sigma_z + \frac{\omega_1}{2}\left(\sigma_x \cos(\omega t) + \sigma_y \sin(\omega t)\right),$$

where ω_1 depends on the x-y plane component B_1 of the magnetic field, $\omega_1 = -B_1\gamma$. To solve the Schrödinger equation, we put $|\psi(t)\rangle$ in a "frame" rotating with the magnetic field around the z axis at frequency ω, $|\phi(t)\rangle = e^{i\omega t\sigma_z/2}|\psi(t)\rangle$. With this substitution, the Schrödinger equation (16) becomes

$$i\partial_t|\phi(t)\rangle = (e^{i\omega\sigma_z t/2}He^{-i\omega\sigma_z t/2} - \frac{\omega}{2}\sigma_z)|\phi(t)\rangle. \tag{17}$$

Using properties

$$\begin{aligned} e^{i\omega\sigma_z t/2}\sigma_z e^{-i\omega\sigma_z t/2} &= \sigma_z, \\ e^{i\omega\sigma_z t/2}\sigma_x e^{-i\omega\sigma_z t/2} &= \sigma_x\cos(\omega t) - \sigma_y\sin(\omega t), \\ e^{i\omega\sigma_z t/2}\sigma_y e^{-i\omega\sigma_z t/2} &= \sigma_x\sin(\omega t) + \sigma_y\cos(\omega t), \end{aligned} \tag{18}$$

we obtain

$$i\partial_t|\phi(t)\rangle = \left(\frac{\omega_0 - \omega}{2}\sigma_z + \frac{\omega_1}{2}\sigma_x\right)|\phi(t)\rangle,$$
$$|\phi(t)\rangle = e^{-i((\omega_0-\omega)\sigma_z/2 + \omega_1\sigma_x/2)t}|\phi(0)\rangle. \tag{19}$$

We know from (9) that this is a rotation around the axis

$$\mathbf{n} = \frac{1}{\sqrt{1 + (\frac{\omega_1}{\omega_0-\omega})^2}}\left(\mathbf{e}_z + \frac{\omega_1}{\omega_0-\omega}\mathbf{e}_x\right). \tag{20}$$

An important case is $\omega_0 = \omega$, also called the *resonance* case where its name came from the zero denominator in (20). By (19), we see that a relatively weak transverse magnetic field causes a rotation around the x axis:

$$|\psi(t)\rangle = e^{-i\omega\sigma_z t/2}|\phi(t)\rangle = e^{-i\omega_0 t\sigma_z/2}e^{-i\omega_1 t\sigma_x/2}|\phi(0)\rangle = Z_\theta X_\beta|\psi(0)\rangle, \quad (21)$$

where $X_\beta = e^{-i\omega_1 t\sigma_x/2}$, $\beta = \omega_1 t$. By applying another $Z_{-\theta}$, we obtain a rotation X_β as desired. Since the frequency of the precession is in radio frequency band, the field applied is called an *RF pulse*.

When $|\omega_0 - \omega| \gg \omega_1$, the rotation axis direction is almost along $\mathbf{z}$ and the RF pulse has no effect on it:

$$|\psi(t)\rangle = e^{-i\omega\sigma_z t/2}|\phi(t)\rangle \approx e^{-i\omega_0 t\sigma_z/2}|\psi(0)\rangle = Z_{\omega_0 t}|\psi(0)\rangle,$$

thus we can tell one qubit from another because their resonance frequencies are designed to be different. There are still cases where the difference of resonance frequencies between spins is not large enough. The RF pulse may cause similar rotations on all those spins. To avoid or at least minimize it, a *soft* pulse is applied instead of the so called *hard* pulse. It is a pulse with longer time span and weaker magnetic field, in other word, a smaller ω_1. This strategy makes these "close" qubits fall into the $|\omega_0 - \omega| \gg \omega_1$ case.

If we change the magnetic field to

$$\mathbf{B} = B_0\mathbf{e}_z + B_1(\mathbf{e}_x\cos(\omega_0 t + \alpha) + \mathbf{e}_y\sin(\omega_0 t + \alpha)), \quad (22)$$

the Hamiltonian will become

$$H = \frac{\omega_0}{2}\sigma_z + \frac{\omega_1}{2}(\sigma_x\cos(\omega_0 t + \alpha) + \sigma_y\sin(\omega_0 + \alpha)) \quad (23)$$

where ω_1 is defined as before. The RF field is almost the same as (14) in the resonance case except a phase shift. Using the same rotation frame as before with $\omega = \omega_0$, we obtain

$$i\partial_t|\phi(t)\rangle = \frac{\omega_1}{2}(\sigma_x\cos(\alpha) + \sigma_y\sin(\alpha))|\phi(t)\rangle, \quad (24)$$

after simplification. After time duration t, the new system state is given as

$$|\phi(t)\rangle = e^{-i\frac{\omega_1}{2}(\sigma_x\cos(\alpha)+\sigma_y\sin(\alpha))t}|\phi(0)\rangle, \quad (25)$$

and the evolution operator can be computed using (9) as

$$U_{\theta/2,\alpha} = e^{-i\frac{\omega_1}{2}(\sigma_x\cos(\alpha)+\sigma_y\sin(\alpha))t}$$
$$= \begin{bmatrix} \cos(\frac{\theta}{2}) & -i\sin(\frac{\theta}{2})e^{-i\alpha} \\ -i\sin(\frac{\theta}{2})e^{i\alpha} & \cos(\frac{\theta}{2}) \end{bmatrix}, \quad (26)$$

where $\theta = \omega_1 t$. This is a one-qubit rotation operator, and sometimes is called a Rabi rotation gate. When $\alpha = \pi/2$,

$$U_{\theta/2,\pi/2} = \begin{bmatrix} \cos(\frac{\theta}{2}) & -\sin(\frac{\theta}{2}) \\ \sin(\frac{\theta}{2}) & \cos(\frac{\theta}{2}) \end{bmatrix}$$
$$= Y_\theta. \quad (27)$$

We have achieved a y-rotation operator just by adding a phase shift to the RF field.

Two-qubit gates

The construction of a two-qubit gate requires the coupling of two spins. In a liquid sample of NMR, *J-coupling* is the dominating coupling between spins. Under the assumption that the resonance frequency difference between the coupled spins is much larger than the strength of the coupling (a so-called weak coupling regime), the total Hamiltonian of a two spin system without transverse field may be given as

$$H = \frac{1}{2}\omega_1\sigma_z^1 + \frac{1}{2}\omega_2\sigma_z^2 + \frac{1}{2}J\sigma_z^1\sigma_z^2, \tag{28}$$

where ω_i is the frequency corresponding to spin i, σ_z^i is the z projection operator of spin i, for $i = 1, 2$, and J is the coupling coefficient. Take the chloroform in Fig. 6 for example [14, 80]. In a 11.7T magnetic field, the precession frequency of ^{13}C is about $2\pi \times 500$MHz and the precession frequency of proton is about $2\pi \times 125$MHz. The coupling constant J is about $2\pi \times 100$Hz. Here we set $B_1 = 0$, which means no transverse magnetic field is applied and those terms such as σ_x, σ_y do not appear. The remaining terms in the Hamiltonian only contains operators σ_z^1 or σ_z^2, which are commutative. Thus, we can obtain the eigenstates and eigenvalues of this two-spin system and we map the set of eigenstates to the standard basis of $\mathbf{C}^4$, as follows:

$$|00\rangle = \begin{bmatrix} 1 \\ 0 \\ 0 \\ 0 \end{bmatrix}, \ |01\rangle = \begin{bmatrix} 0 \\ 1 \\ 0 \\ 0 \end{bmatrix}, \ |10\rangle = \begin{bmatrix} 0 \\ 0 \\ 1 \\ 0 \end{bmatrix}, \ |11\rangle = \begin{bmatrix} 0 \\ 0 \\ 0 \\ 1 \end{bmatrix}; \tag{29}$$

$$\begin{aligned}
H|00\rangle &= k_{00}|00\rangle, \ k_{00} = \tfrac{1}{2}\omega_1 + \tfrac{1}{2}\omega_2 + \tfrac{1}{2}J; \\
H|01\rangle &= k_{01}|01\rangle, \ k_{01} = \tfrac{1}{2}\omega_1 - \tfrac{1}{2}\omega_2 - \tfrac{1}{2}J; \\
H|10\rangle &= k_{10}|10\rangle, k_{10} = -\tfrac{1}{2}\omega_1 + \tfrac{1}{2}\omega_2 - \tfrac{1}{2}J; \\
H|11\rangle &= k_{11}|11\rangle, k_{11} = -\tfrac{1}{2}\omega_1 - \tfrac{1}{2}\omega_2 + \tfrac{1}{2}J.
\end{aligned} \tag{30}$$

Since the matrix is diagonal, the evolution of this two-spin system can be easily derived as

$$|\psi(t)\rangle = e^{-iHt}|\psi(0)\rangle = \begin{bmatrix} e^{-ik_{00}t} & & & \\ & e^{-ik_{01}t} & & \\ & & e^{-ik_{10}t} & \\ & & & e^{-ik_{11}t} \end{bmatrix} |\psi(0)\rangle. \tag{31}$$

We can also rewrite the one qubit rotation operators for this two $\frac{1}{2}$-spin system in matrix form with respect to the same basis:

$$Z_{\pi/2}^1 = \begin{bmatrix} e^{-i\pi/4} & & & \\ & e^{-i\pi/4} & & \\ & & e^{i\pi/4} & \\ & & & e^{i\pi/4} \end{bmatrix}, \tag{32}$$

$$Z_{-\pi/2}^2 = \begin{bmatrix} e^{i\pi/4} & & & \\ & e^{-i\pi/4} & & \\ & & e^{i\pi/4} & \\ & & & e^{-i\pi/4} \end{bmatrix}, \tag{33}$$

$$Y_{\pi/2}^2 = \frac{\sqrt{2}}{2} \begin{bmatrix} 1 & -1 & & \\ 1 & 1 & & \\ & & 1 & -1 \\ & & 1 & 1 \end{bmatrix}, \tag{34}$$

$$Y_{-\pi/2}^2 = \frac{\sqrt{2}}{2} \begin{bmatrix} 1 & 1 & & \\ -1 & 1 & & \\ & & 1 & 1 \\ & & -1 & 1 \end{bmatrix}, \tag{35}$$

where Z_θ^i is the rotation operator for spin i with angle θ around the z axis while keeping the other spin unchanged, and all Y_θ^i are similarly defined operators about the y axis; see (12). A careful reader may raise issues about the one-qubit gate we have obtained in subsection 2.4 because the coupling between two qubits always exists and has not been considered. We need to turn off the coupling when we only want to operate one spin but the coupling is non-negligible. This is in fact one of the major characteristic difficulties associated with the NMR quantum computing technology. A special technology called *refocusing* is useful. It works as follows. We apply a soft π pulse on the spare spin that we don't want to change at the middle point of the operation time duration while we are working on the target spin. The effect is that the coupling before the pulse cancels the one after the pulse, so the result of no-coupling is achieved. Another π pulse will be needed to turn the spin back. All pulses are soft.

This technology is so important that we now state it here as a theorem.

Theorem 2.3 *Let $H = \frac{\omega_1}{2}\sigma_z^1 + \frac{J}{2}\sigma_z^1\sigma_z^2 + A$ be a given Hamiltonian, where A is a Hamiltonian that does not act on spin 1 and commutes with σ_z^2. Then the evolution operators of A and H satisfy*

$$e^{-iAt} = -X_\pi^1 e^{-iHt/2} X_\pi^1 e^{-iHt/2}, \tag{36}$$

i.e., the collective evolution of the quantum system with Hamiltonian H and additional two X_π^1-pulses at the middle and the end of the time duration, equals that of a system with Hamiltonian A (up to a global phase shift π, or a factor -1). $\square$

Proof. Assume that the time duration is t and denote U for

$$U = X_\pi^1 e^{-iHt/2} X_\pi^1 e^{-iHt/2}. \tag{37}$$

Note that $X_\pi^1 = e^{-i\frac{\pi}{2}\sigma_x^1}$ and it commutes with A which contains no operators acting on spin 1, thus

$$U = X_\pi^1 e^{-i(\frac{\omega_1}{2}\sigma_z^1 + \frac{J}{2}\sigma_z^1\sigma_z^2)\frac{t}{2}} X_\pi^1 e^{-i(\frac{\omega_1}{2}\sigma_z^1 + \frac{J}{2}\sigma_z^1\sigma_z^2)\frac{t}{2}} e^{-iAt}. \tag{38}$$

It suffices to prove that the part before e^{-iAt} satisfies

$$B = X_\pi^1 e^{-i(\frac{\omega_1}{2}\sigma_z^1 + \frac{J}{2}\sigma_z^1\sigma_z^2)\frac{t}{2}} X_\pi^1 e^{-i(\frac{\omega_1}{2}\sigma_z^1 + \frac{J}{2}\sigma_z^1\sigma_z^2)\frac{t}{2}} = -I. \tag{39}$$

We first check the effect of B on the four basis vector. We have

$$
\begin{aligned}
B|11\rangle &= X_\pi^1 e^{-i(\frac{\omega_1}{2}\sigma_z^1 + \frac{J}{2}\sigma_z^1\sigma_z^2)\frac{t}{2}} X_\pi^1 e^{-i(\frac{\omega_1}{2}\sigma_z^1 + \frac{J}{2}\sigma_z^1\sigma_z^2)\frac{t}{2}}|11\rangle \\
&= e^{-i\frac{-\omega_1+J}{4}t}(-i)X_\pi^1 e^{-i(\frac{\omega_1}{2}\sigma_z^1 + \frac{J}{2}\sigma_z^1\sigma_z^2)\frac{t}{2}}|01\rangle \\
&= (-i)e^{-i\frac{-\omega_1+J}{4}t} X_\pi^1 e^{-i\frac{\omega_1-J}{4}t}|01\rangle \\
&= (-i)^2|11\rangle \\
&= -|11\rangle,
\end{aligned} \tag{40}
$$

$$
\begin{aligned}
B|01\rangle &= X_\pi^1 e^{-i(\frac{\omega_1}{2}\sigma_z^1 + \frac{J}{2}\sigma_z^1\sigma_z^2)\frac{t}{2}} X_\pi^1 e^{-i(\frac{\omega_1}{2}\sigma_z^1 + \frac{J}{2}\sigma_z^1\sigma_z^2)\frac{t}{2}}|01\rangle \\
&= e^{-i\frac{\omega_1-J}{4}t}(-i)X_\pi^1 e^{-i(\frac{\omega_1}{2}\sigma_z^1 + \frac{J}{2}\sigma_z^1\sigma_z^2)\frac{t}{2}}|11\rangle \\
&= (-i)e^{-i\frac{-\omega_1+J}{4}t} X_\pi^1 e^{-i\frac{-\omega_1+J}{4}t}|11\rangle \\
&= (-i)^2|01\rangle \\
&= -|01\rangle,
\end{aligned} \tag{41}
$$

and similarly,

$$
\begin{aligned}
B|10\rangle &= -|10\rangle, \\
B|00\rangle &= -|00\rangle.
\end{aligned} \tag{42}
$$

In the computation above, we have used the fact that X_π^1 has no effect on the second spin and the four basis vectors $|00\rangle$, $|01\rangle$, $|10\rangle$ and $|11\rangle$ are the eigenstates of the operator $\frac{\omega_1}{2}\sigma_z^1 + \frac{J}{2}\sigma_z^2\sigma_z^1$. The result shows that $B = -I$, and we are done. $\qquad\square$

When the Hamiltonian is given in the form as (28), the above theorem tells us that both the chemical shift evolution (precession) and the J-coupling effect on spin 1 are removed and only the term $\frac{\omega_2}{2}\sigma_z^2$ remains. We obtain a z-rotation of spin 2 while freezing spin 1. By combining it with several hard pulses, we can also achieve any arbitrary rotation on spin 2 with the motion of spin 1 frozen [70]. Similar computation shows that a hard π pulse applied at the middle point of the time duration cancels the chemical shift evolution of both spins. This can be seen by checking the identity

$$e^{-iHt/2} X_\pi^1 X_\pi^2 e^{-iHt/2} = \begin{bmatrix} & & & e^{-iJt/2} \\ & & e^{iJt/2} & \\ & e^{iJt/2} & & \\ e^{-iJt/2} & & & \end{bmatrix}. \tag{43}$$

Another hard π pulse can rotate two spins back, so we have achieved an evolution which has only the J-coupling effect, denoted by $\mathbb{Z}_\theta$:

$$\mathbb{Z}_\theta = \begin{bmatrix} e^{-i\theta/2} & & & \\ & e^{i\theta/2} & & \\ & & e^{i\theta/2} & \\ & & & e^{-i\theta/2} \end{bmatrix},$$

and when $\theta = \pi/2$,

$$\mathbb{Z}_{\pi/2} = \begin{bmatrix} e^{-i\pi/4} & & & \\ & e^{i\pi/4} & & \\ & & e^{i\pi/4} & \\ & & & e^{-i\pi/4} \end{bmatrix}. \tag{44}$$

Although we give only an example of the 2-qubit system in the above, the reader should note that a general method is available to reserve only the couplings wanted while keeping all the others cancelled for multi-qubit systems [56, 68, 70]. Combining operators in (32) through (35) and (44), we can now construct a CNOT gate as in Fig. 8 which includes four one-qubit $\pi/2$ rotations around y or z axes and one two-qubit $\pi/2$ rotation. The total operator, denoted by CN, can be computed as

$$CN = Z^1_{\pi/2} Y^2_{-\pi/2} Z^2_{-\pi/2} \mathbb{Z}_{\pi/2} Y^2_{\pi/2} = e^{-\frac{\pi}{4}i} \begin{bmatrix} 1 & & & \\ & 1 & & \\ & & 0 & 1 \\ & & 1 & 0 \end{bmatrix}, \tag{45}$$

which is a CNOT gate up to a phase of $-\pi/4$ [80].
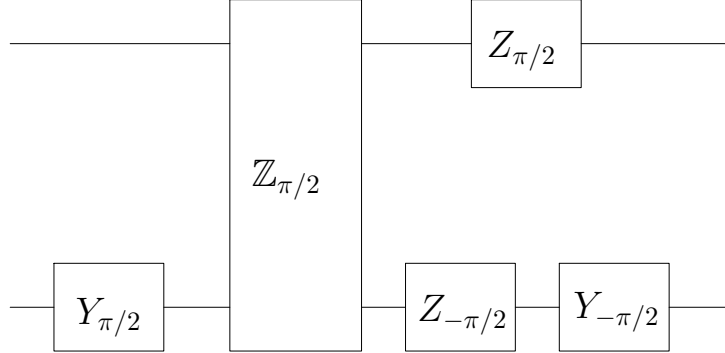
Fig. 8. The quantum circuit used to realize a quantum controlled-not gate.

We have shown how to construct one-qubit gates and the two-qubit CNOT gate using the NMR technology. The simple pulse design works fine in ideal

situations. In practice, errors arise from various factors. Decoherence causes the lost of quantum information with time. Thus, all operations should be completed within a short time, roughly constrained by the energy relaxation time T_1 and the phase randomization time T_2. Again, take the chloroform for an example. For protons, $T_1 \approx 7\text{sec}$ and $T_2 \approx 2\text{sec}$; for carbons, $T_1 \approx 16\text{sec}$ and $T_2 \approx 0.2\text{sec}$ [14, 80]. The pulses have to be short enough so that all the pulses can be jammed in the time window. Ideally, a pulse can be completed quite fast, but this may incur undesirable rotations in other qubits because the frequency band width is inversely proportional to the time length of the pulse. A shorter and stronger pulse will have a wider frequency band that may cover the resonance frequency of another spin, called *cross-talking*. It should also be noted that both T_1 and T_2 are defined and measured in simplified situation, and they can only be used as an approximation of the decoherence rate for the quantum computation. Coupling is also a problem which makes the pulse design much more complicated. Finally, any experimental facility is not perfect, which may introduce more errors. Typical error resources include *inhomogeneities in the static and RF field*, *pulse length calibration errors*, *frequency offsets*, and *pulse timing/phase imperfections*.

If the quantum circuit can be simplified and the number of gates needed is reduced, the requirements on the pulses can be alleviated. Mathematicians are looking for methods to find time-optimal pulse sequences [41, 58, 59, 97], with the goal of finding the shortest path between the identity and a point in the space of **SU**(n) allowed by the system and the control Hamiltonians. Besides that, NMR spectroscopists have already developed advanced pulse techniques to deal with system errors such as cross-talking and coupling. They turn out to work well and are now widely used in NMR quantum computation. Such techniques include composite pulses [19, 34, 69, 53, 54, 106] and pulse shaping. The latter consists mainly of two methods: phase profiles [87] and amplitude profiles [37, 64].

2.5 Initialization

An NMR sample eventually will go into its equilibrium state when no RF pulse is applied for a long time. Then the density matrix is proportional to $e^{-H/kT}$, according to the Boltzmann distribution, where $k = 1.381 \times 10^{-23}\text{J/K}$ and T is the absolute temperature. Normally, the environment temperature is far larger than the energy difference between the up and down states of the spin, and H/kT is very small, about 10^{-4}. We also make the assumption that the coupling terms are small enough compared with the resonant frequency, thus we can make a reasonable approximation of the equilibrium state density matrix of a system with n spins:

$$\rho_{eq} = \frac{e^{-H/kT}}{tr(e^{-H/kT})} \approx I - \frac{1}{kT}(\epsilon_1 \sigma_z^1 + \epsilon_2 \sigma_z^2 + \cdots + \epsilon_n \sigma_z^n). \qquad (46)$$

In the four operators appearing in the density matrix (5), only those with zero traces can be observed in NMR. The operator I_0 is invisible, and moreover, it remains invariant under any unitary similarity transformation. Therefor, we only need to take care of the zero-trace part of the initial density matrix, noting that only that part (called deviation) is effective. Most algorithms prefer an initial state such as

$$\rho_0 = \frac{1-\epsilon}{2^n} I + \epsilon |00\cdots 0\rangle\langle 0\cdots 00|,$$

which is an example of the so called *pseudo-pure* states, corresponding to the pure state $|00\cdots 0\rangle$.

To initialize the system to a pseudo-pure state as above, we may use a scheme called *averaging*. Let us explain this for a 2-spin system. Suppose we have three 2-spin subsystems with density matrices

$$\rho_1 = \begin{bmatrix} a & 0 & 0 & 0 \\ 0 & b & 0 & 0 \\ 0 & 0 & c & 0 \\ 0 & 0 & 0 & d \end{bmatrix}, \quad \rho_2 = \begin{bmatrix} a & 0 & 0 & 0 \\ 0 & c & 0 & 0 \\ 0 & 0 & d & 0 \\ 0 & 0 & 0 & b \end{bmatrix}, \quad \rho_3 = \begin{bmatrix} a & 0 & 0 & 0 \\ 0 & d & 0 & 0 \\ 0 & 0 & b & 0 \\ 0 & 0 & 0 & c \end{bmatrix}, \tag{47}$$

respectively, where a, b, c, and d are nonnegative, and $a+b+c+d=1$. These are three diagonal matrices with three of their diagonal elements in cyclic permutation.

Now, we mix these three subsystems together (for n-qubit system, we may have $2^n - 1$ subsystems) and assume that the three subsystems have the same signal scale. Because the readout is linear with respect to the initial state, we are in fact working on a system with an effective initial density matrix

$$\frac{1}{3} \sum_{i=1}^{3} \rho_i = \frac{1}{3} \begin{bmatrix} 3a & & & \\ & b+c+d & & \\ & & b+c+d & \\ & & & b+c+d \end{bmatrix}$$

$$= \frac{b+c+d}{3} I + \frac{1}{3} \begin{bmatrix} 4a-1 & 0 & 0 & 0 \\ 0 & 0 & 0 & 0 \\ 0 & 0 & 0 & 0 \\ 0 & 0 & 0 & 0 \end{bmatrix}, \tag{48}$$

which is a pseudo-pure state corresponding to $|00\cdots 0\rangle$.

Various methods have been developed to achieve this effect of averaging. Because ρ_1, ρ_2, and ρ_3 differ only by a permutation of the diagonal elements, a sequence of CNOT pulses can be used to transform one to another. In most cases, we only have one sample, the same algorithm can be repeated on the very sample three times but with different initial states ρ_1, ρ_2, and ρ_3, respectively. At last, after all the three outputs are obtained and added together (average), we achieve the same result as what we will get when the algorithm is employed on a system with the expected initial state $|00\cdots 0\rangle$.

This is called "temporal averaging" [61]. Gradient fields can also be used to divide the sample into different slices in space which are prepared into different initial states, and the averaging is realized spatially, called "spatial averaging" [17]. The number of the experiments and pulses needed grows very large when the number of qubits increases. For example, 9 experiments are combined in order to prepare one pseudo-pure state for a 5-qubit system and 48 pulses are used to form one pseudo-pure state in a 7-qubit system [39] after modifications such as logical labeling [40, 104] and selective saturation [60].

2.6 Measurement

An NMR computer differs from other quantum computers in that it works on an ensemble of spins instead of just a single one. It produces an observable macroscopic signal which can be picked up by a set of coils positioned on the x-y plane, as shown in Fig. 3. The signal measures the change rate of the magnetic field created by a large number of spins in the sample rotating around the z-axis, called *free induction decay* (FID). Due to relaxation, peaks of the Fourier transform of the signal, or spectra, have width. However, we do not need to worry about that since it will not make any substantial difference in our discussion here. One disadvantage is that the readout from NMR is an average of all the possible states, in contrast to most existing quantum algorithms that ask for the occurrence of only a single state. But it is possible for one to modify ordinary quantum algorithms to make NMR results usable.

The magnetization detected by the coil in Fig. 3 is proportional to the trace of the product of the density matrix with $\sigma_+ = \sigma_x + i\sigma_y$:

$$M_x + iM_y = nV\langle\mu_x + i\mu_y\rangle = nV\gamma\hbar Tr(\rho(\sigma_x + i\sigma_y)), \tag{49}$$

where γ is the magnetogyric ratio as in (3) and ρ is the density matrix. When the external RF magnetic field is removed, the density matrix will change according to the system's Hamiltonian as we discussed earlier. If we decompose the density matrix into a sum of product operators as in (5), only I_x and I_y contribute to the readout. We can not "see" the coefficients of I_0 and I_z. Recall (18): if a one-spin system begins from density matrix $\rho_0 = I_0 + \sin\theta\cos\psi I_x + \sin\theta\sin\psi I_y + \cos\theta I_z$, the magnetization will rotate with the resonant frequency as

$$
\begin{aligned}
M_z + iM_y &= C\,Tr(e^{-iHt}\rho_0 e^{iHt}\sigma_+)\\
&= C\,Tr(e^{-iHt}(I_0 + \sin(\theta)\cos(\psi)I_x +\\
&\quad \sin(\theta)\sin(\psi)I_y + \cos(\theta)I_z)e^{iHt}\sigma_+)\\
&= C\,Tr((\sin\theta\cos\psi(\cos(\omega t)I_x + \sin(\omega t)I_y) +\\
&\quad sin\theta\sin\psi(\cos(\omega t)I_y - \sin(\omega t)I_x))\sigma_+)\\
&= C\,\sin\theta\,e^{i(\omega t+\psi)},
\end{aligned}
\tag{50}
$$

where $C = nV\gamma\hbar$. This rotating magnetization will introduce an oscillating electric potential in the receiver coils, which will be processed by a computer

to generate the spectra. Note that the signal is proportional to $\sin \theta$. If an x rotation with angle $\pi/2$ is applied on the spin before the measurement, the magnetization will become

$$M_z + iM_y = \frac{\sqrt{2}}{2} C (\sin \theta \; - \; i \cos \theta) e^{i\omega t}.$$

For simplicity, we have chosen $\psi = 0$. The imaginary part is proportional to the population difference:

$$\cos \theta = \cos^2 \frac{\theta}{2} - \sin^2 \frac{\theta}{2}.$$

Computation of a two-spin system is complicated, so we will only give some partial results here. The purpose is to point out what methodology is used. We will still use the basis given by (29) and the Hamiltonian in (28). The system begins from a density matrix as

$$\rho_0 = \begin{bmatrix} \rho_{11} & \rho_{12} & \rho_{13} & \rho_{14} \\ \rho_{21} & \rho_{22} & \rho_{23} & \rho_{24} \\ \rho_{31} & \rho_{32} & \rho_{33} & \rho_{34} \\ \rho_{41} & \rho_{42} & \rho_{43} & \rho_{44} \end{bmatrix}. \tag{51}$$

The operator σ_+ is a summation of operators from the two subsystems:

$$\sigma_+ = \sigma_+^1 + \sigma_+^2$$
$$= \begin{bmatrix} 0 & 2 & 2 & 0 \\ 0 & 0 & 0 & 2 \\ 0 & 0 & 0 & 2 \\ 0 & 0 & 0 & 0 \end{bmatrix}. \tag{52}$$

The magnetization in the x-y plane is composed of four frequencies:

$$M_x + iM_y = C\, Tr(e^{-iHt} \rho_0 e^{iHt} \sigma_+)$$
$$= C\, (\rho_{31} e^{i(\omega_1 + J)t} + \rho_{42} e^{i(\omega_1 - J)t} + \rho_{43} e^{i(\omega_2 - J)t} + \rho_{21} e^{i(\omega_2 + J)t}). \tag{53}$$

The spectrum has two pairs of peaks, one pair around the precession frequency ω_1, another pair around ω_2. See Fig. 9. The splitting is a result of coupling. If the system have more than two spins, the coupling will split up a peak into up to 2^{n-1} peaks where n is the number of spins. We also combine all the constants in C to make the formula concise. Only four of the elements out of the density matrix appear in this spectrum, so we need to design certain control pulses to move the expected information to these four positions where numbers can be shown via free induction signal. If multi-tests are allowed, theoretically, all the elements of the density matrix can be retrieved [13, 12]. It is also possible to transport the desired information (computational results) to the four positions where the observer can see.
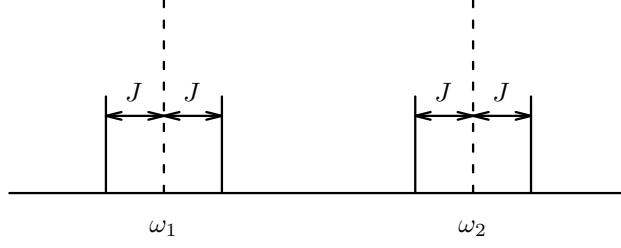
Fig. 9. Simplified stick spectra of a two-qubit molecule. The two dotted lines show two peaks at ω_1 and ω_2, respectively, when no coupling is applied ($J = 0$). After coupling, every peak is split into two small peaks with the intensities reduced to half.

A typical pulse used in reading out is a hard $X_{\pi/2}$ pulse which rotate all the spins about the x-axis with angle $\pi/2$. Let us still use two-spin systems as an example. The operation is the tensor product of two x-rotation operators, i.e., $X_{\pi/2} = X^1_{\pi/2} X^2_{\pi/2}$. The imaginary part of the four effective elements of the density matrix ρ' after the operation, utilizing the fact that the density matrix is Hermitian, are

$$
\begin{aligned}
Im(\rho'_{31}) &= \tfrac{1}{4}(\rho_{33} + \rho_{44} - \rho_{11} - \rho_{22} - 2Im(\rho_{21}) - 2Im(\rho_{34})), \\
Im(\rho'_{42}) &= \tfrac{1}{4}(\rho_{33} + \rho_{44} - \rho_{11} - \rho_{22} + 2Im(\rho_{21}) + 2Im(\rho_{34})), \\
Im(\rho'_{43}) &= \tfrac{1}{4}(\rho_{22} + \rho_{44} - \rho_{11} - \rho_{33} + 2Im(\rho_{31}) + 2Im(\rho_{24})), \\
Im(\rho'_{21}) &= \tfrac{1}{4}(\rho_{22} + \rho_{44} - \rho_{11} - \rho_{33} - 2Im(\rho_{31}) - 2Im(\rho_{24})).
\end{aligned}
\tag{54}
$$

Find the sum of $Im(\rho'_{31})$ and $Im(\rho'_{42})$ and that of $Im(\rho'_{43})$ and $Im(\rho'_{21})$:

$$
\begin{aligned}
Im(\rho'_{31} + \rho'_{42}) &= -\tfrac{1}{2}(\rho_{11} + \rho_{22} - \rho_{33} - \rho_{44}), \\
Im(\rho'_{43} + \rho'_{21}) &= -\tfrac{1}{2}(\rho_{11} - \rho_{22} + \rho_{33} - \rho_{44}).
\end{aligned}
\tag{55}
$$

Because what the coils pick up is the change rate of the magnetic field rather than the magnetic field itself, the imaginary part we have listed above is reflected in the real part of the spectra. The computation above shows that the sum of the real parts of each pair of peaks in the spectra is proportional to the population difference between the spin-up and the spin-down states of the corresponding spin.

3 Solid state NMR

Liquid NMR, discussed in Section 2, has several constrains that make a liquid NMR quantum computer *not scalable*. At first, as the result of the pseudo-pure state preparation, the signal-noise ratio decreases exponentially when the number of qubits increases, limiting its ability to realize more qubits. Another difficulty arises when we want to control the system as accurately

as desired. Because the range of the chemical shift is limited by nature, the number of qubits represented by the same type of nuclei, such as carbon, is constrained as the resonance frequency gaps between any two qubits must be large enough so that we can distinguish the qubits easily and control them with great precision. It is estimated that a quantum computer realized by liquid state NMR can has at most 10 to 20 qubits.

Solid state NMR has the potential to overcome many of the problems of its liquid state counterpart as in the preceding paragraph. These advantages are derived partly from the lack of motion of the molecules and partly from the ability to cool to low temperatures. As with many potential solutions, there are tradeoffs to consider. Here we summarize:

1) At low temperatures, near or below that of liquid helium, it is possible to initialize electron spins using the thermal Boltzman distribution. Nuclear spins do not become significantly oriented until much lower temperatures because of their 1000 times lower energies, but there are existing pulse RF sequences that can transfer an electron spin orientation to nearby nuclear spins using their mutual spin-spin interaction. In principle, this solves the problem of qubit initialization. In practice, the thermal initialization process can be slow since it depends on the electron spin population lifetime. It is possible to find systems with short electron spin lifetimes, but this will tend to result faster decoherence of the nuclear spins, since they must be coupled to the electron in order to initialize in the first place.

2) Because the molecules in a solid are usually not tumbling, the dipole coupling between nearby spins does not average out. This has the advantage of making multi-qubit gates faster, since the dipole coupling is much larger than the scalar coupling. The orientation dependent chemical shifts also do not average out, in principle making individual qubits easier to address so that more qubits can be used. Here, it should be noted that custom molecules containing electron spins [109] can be used to enhance this effect. There is a tradeoff to consider, in that the faster interaction with nearby spins provided by dipole coupling can also lead to faster decoherence times.

3) Spin lifetimes in solids can be much longer than in liquids. Lack of molecular motion eliminates the spatial diffusion of spins which is a problem in liquid NMR for times in the range of milliseconds or longer [32]. Phonons can cause decoherence in solids at room temperature, but this can be strongly suppressed at temperatures achievable in liquid helium. It is not unusual to see spin population lifetimes of minutes in solids, especially at low temperatures. Unfortunately, spin coherence times are usually somewhat shorter due to dephasing caused by mutual spin flips through the strong dipole coupling. To eliminate this decoherence mechanism, there are two main approaches. One is to disperse the active molecule, as a dopant in a spin-free host. Actually the host does not need to be completely spin free provided its spins are far enough off resonance with those of the active molecule. Another technique is to use stoichiometric materials consisting of relatively large unit cells contain-

ing many spin-free atoms. The idea for both these approaches is to keep the active nuclei relatively far apart, except for nearest neighbors.

Beside above differences, nuclei with non-zero spin in *solid state* can also be used for quantum computation [65] and manipulated similar to the liquid state NMR. Because all the nuclei are fixed in space, a static magnetic field with strong gradient in one direction separates the nuclei into different layers along the direction. Every layer of nuclei can be regarded as a qubit and the qubits have different resonance frequencies as the magnetic field is different from one layer to another. Readout also can be made to take advantage of the bulk quantum computer much like the liquid NMR. Signal is picked up using methods like magnetic resonance force microscopy.

There are two types of methods to make such nuclei arrangement. Crystal, such as cerium-monophosphide (CeP), is a natural choice, where the 1/2 spin ^{31}P nuclei form periodical layers in the crystal with inter-layer distance about 12Å [43, 114]. Another method is to grow a chain of ^{29}Si that has 1/2 spin along the static field direction on a base of pure ^{28}Si or ^{30}Si which are both 0 spin nuclei [1, 66]. The last one combines the mature crystal growth and processing technology for silicon from the semiconductor industry. Liquid crystal [115] or solid-state sample [67] are also candidates for realizing NMR quantum computer.

Recently, there has been considerable progress made in the area of *optically addressed spins in solids*. As a result some highly scalable designs have recently come forward that have the potential to eliminate all of the limitations of NMR. Aside from potentially solving NMR's problems, optical addressing has the important advantage that it would provide an interface between spin qubits and optical qubits, which is essential to interface with existing quantum communication systems, and for quantum networking in general.

Optically addressed spins are better known in the literature as *spectral hole burning* (SHB) materials [78]. Most of these are dopant-host systems that exhibit strong zero-phonon optical absorption lines at low temperature. Due to the inherent inhomogeneity of dopant-host systems it is often found that this optical zero-phonon linewidth is much larger than that of the individual atoms. Furthermore, when these transitions are excited with a narrowband laser, the resonant atoms can be optically pumped into a different ground state, making the material more transparent at the laser frequency. This is known as burning a spectral hole, hence the name *SHB*. In many SHB materials, the optical pumping is into different ground state spin sublevels, and hence the hole burning process can initialize spin qubits, as illustrated in Fig. 10. This type of spin qubit initialization can be much faster than Boltzmann initialization, especially in spin systems with long spin population lifetimes, since the tradeoff between spin lifetime and initialization speed is removed.

In addition to optical initialization of spins, the hole burning process can also be used to readout the spin state of the qubits. This happens when the quantum algorithm returns some of the spin qubits to the state that was initially emptied by the laser, resulting in a temporary increase in laser
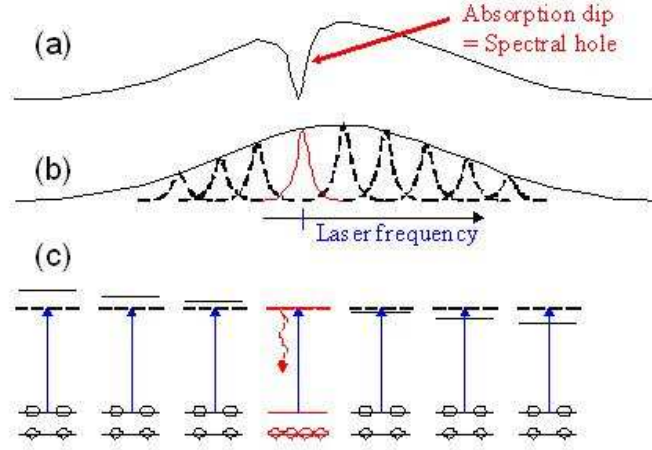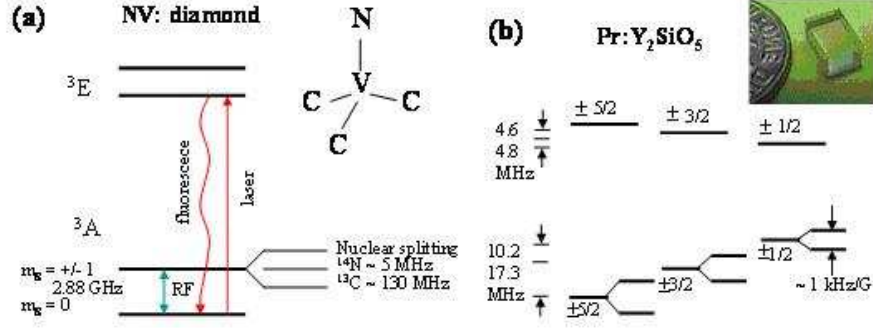
Fig. 10. (a) The signature of spectral hole burning is a narrowband dip in the optical absorption spectrum. (b) This dip occurs when an optical laser bleaches out an ensemble of atoms at a particular transition frequency. (c) In the case when bleaching is due to spin sublevel optical pumping, it can be used to initialize qubits.

absorption and/or fluorescence that is proportional to the final population of this spin state. Of course, the readout process also re-initializes, so one must take care to work with a large enough ensemble to achieve the desired readout fidelity. In general, optical readout is orders of magnitude more sensitive than the typical NMR coil, and so it is possible to work with small ensembles consisting of very dilute dopant-host systems that can have very long spin coherence lifetimes.

Spin qubit coherence lifetime in SHB materials can be lengthened by a variety of techniques. In dilute dopant-host systems, the choice of a spin-free or low-spin host has the largest benefit. Examples include praseodynium [48] or europium [30] doped in a yttrium-silicate host ($Pr : YSO$ or $Eu : YSO$) and nitrogen-vacancy [108] (NV) color centers doped in diamond, see Fig. 11. In $Pr : YSO$ only the yttrium host nuclei have spin but the magnetic moment is very weak. In NV diamond, the only host spins are 1% abundant ^{13}C which can be virtually eliminated with isotopically pure material. In dopant-host systems dephasing due to host spins are reduced by the so-called *frozen core effect* [99], wherein the magnetic field generated by the active (qubit) spin system tunes nearby host nuclei out of resonance with the rest of the crystal up to a distance which defines the frozen core radius. This suppresses the energy conserving mutual spin flips that are the main source of spin decoherence.

In $Pr : YSO$ the spin Hamiltonian is given by [74]:

$$H = \mathbf{B} \cdot \left(g_J^2 \mu_B^2 \overleftrightarrow{\Lambda} \right) \cdot \mathbf{B} + \mathbf{B} \cdot \left(\gamma_N \overleftrightarrow{E} + 2 A_J g_J \mu_B \overleftrightarrow{\Lambda} \right) \cdot \mathbf{I} + \mathbf{I} \cdot \left(A_J^2 \overleftrightarrow{\Lambda} + \overleftrightarrow{T}_Q \right) \cdot \mathbf{I},$$

$$(56)$$

Fig. 11. (a) Spin sublevels of nitrogen-vacancy (NV) color center in diamond. (b) Spin sublevels of Pr:YSO.

where the tensor $\overleftrightarrow{\Lambda}$ is given by

$$\Lambda_{\alpha\beta} = \sum_{n=1}^{2J+1} \frac{\langle 0|J_\alpha|n\rangle\langle n|J_\beta|0\rangle}{\Delta E_{n,0}}, \tag{57}$$

$\overleftrightarrow{E}$ is the 3×3 identity matrix, $\mathbf{B}$ is the magnetic field, and $\mathbf{I}$ is the nuclear spin vector, g_J is the Landé coefficient g, γ_N is the nuclear magnetogyric ratio, A_J is the hyperfine interaction. The term $\mathbf{I}\cdot\overleftrightarrow{T}_Q\cdot\mathbf{I}$ described the nuclear electric quadrupole interaction and $A_J^2\mathbf{I}\cdot\overleftrightarrow{\Lambda}\cdot\mathbf{I}$ is the second order magnetic hyperfine or pseudoquadrupole interaction.

Recently, a spin coherence lifetime of 1/2 minute has been observed in $Pr:YSO$ [35]. This impressive result is made possible by combining two techniques. The first technique involves magnetically tuning the qubit spin to a level anti-crossing [36]. These are common in systems with spin 1 or larger. Near such an anti-crossing there is no first order magnetic Zeeman shift. Consequently, spin flips of nearby host and active spins, which ordinarily introduce coherence by perturbing the local magnetic field of the qubit, no longer have a first order effect. The complication is that the magnetic field is a vector so that the level anti-crossing must exist in all three directions. Nonetheless such global level-crossings were found in $Pr:YSO$ and were used to lengthen the qubit spin coherence lifetime by orders of magnitude. More importantly, the residual spin decoherence was found to decay as a quadratic exponential in time, meaning it decays as $e^{-(t/\tau)^2}$. This is critical because most quantum error correction schemes require the short-time decay to be slower than the usual linear exponential decay. Since this condition was satisfied in $Pr:YSO$, a version of bang-bang error correction was successfully applied to give the observed half minute coherence times.

Manipulation of spin qubits in SHB materials is generally done using RF coils similar to those used in liquid NMR. Recently, optical Raman transitions

have been explored as an alternative to this, in which case the spin-qubits are manipulated by lasers instead of an RF coil. The advantages of this are two-fold. First, the gate time can be made faster because it depends on the optical Rabi frequency, rather than that of the spin transition. One reason for this is that spin transitions are generally magnetic dipole allowed transitions, whereas optical transitions are often electric dipole allowed. Another reason is that it is often easier to insert strong laser fields into a cryostat than strong RF fields. Second, the selectivity of qubit excitation can be improved considerably because only spins with the correct optical transition frequency and spin transition frequency are manipulated. Additional spatial selectivity exists because the optical laser beams can be focused down to microns, and only the illuminated part undergoes qubit manipulations. This is especially important for algorithms like those designed for a Type II quantum computer, see Section 5.

The real power of optically addressed NMR lies in multi-qubit manipulations. The optical "handle" allows several options to increase scalability. First, the relatively long range of optical interactions frees NMR from the restrictions imposed by near-neighbor interactions. An example of this is an ensemble-based two qubit gate demonstration in $Eu : YSO$ involving ions separated by 100 nanometers [76], which is orders of magnitude larger than distances required by conventional NMR. In this demonstration, a series of optical pulses refocuses a "target" optical qubit with a different phase depending on whether the "control" qubit is excited or not. Since these qubits are defined only by their transition frequency, neither the exact location nor number of spins located in between is important. This demonstration also illustrates the interesting fact that optical transitions in some SHB materials have a coherence lifetime that is similar to that of many room temperature NMR transitions.

In principle, long range optical interactions such as in the $Eu : YSO$ example are scalable. In practice, however, the $Eu : YSO$ demonstration experiment is not very scalable because well-defined pairs of qubits must be distilled out of a random ensemble [92], and this incurs an exponential penalty with number of qubits. To make this technique more scalable one approach would be to apply it to special solid state pseudo-molecules. These pseudo-molecules exist in a number of stoichiometric crystals, the most interesting of which are those containing europium, for example $EuVO_4$ or Eu_2O_3 because of their narrow optical transitions at low temperatures [46, 75]. In these pseudo-molecules, localized defects have a large effect on the optical transition frequency of the Eu ions. Up to 50 optical transitions can be easily resolved in these materials. Assuming that all the defects are identical, each optical transition would correspond to a Eu spin system in a well-defined location near the defect center, thereby producing a pseudo-molecule. By using the long range optical coupling demonstrated in $Eu : YSO$, one could in principle construct up to a 50 qubit quantum computer without most of the usual scaling limitations of NMR.

To achieve scalability beyond 100 qubits, single spin manipulation is preferred. The excitation and especially detection of single spins in a solid is a very active area of research. Much of this research is based on a proposal to build a quantum computer using qubits consisting of nuclear spins of a phosphorous atom implanted in a silicon host [57], see Fig. 12. ^{31}P nuclei in spin-free ^{28}Si have a spin population lifetime on the order of hours at ultra-cold temperatures, with coherence lifetimes on the scale of 10's of milliseconds so far. Single qubit manipulations would be done with the usual NMR pulse sequences. However, to avoid driving all the qubits at once, an off resonant RF field is applied and the active qubit is tuned into resonance when desired by using the interaction with its electron spin. The electron spin in turn is controlled by distorting the P electron cloud with a voltage applied to a nearby gate, called the A-electrode. To achieve two-qubit logic, the electron clouds of two neighboring P atoms are overlapped using a J-electrode. The resulting exchange interaction between the two electrons can then be transferred to the P nuclei using RF and/or gate pulse sequences. Since the P atom has electron spin, Boltzmann initialization can be used, though a number of faster alternatives such as spin injection are being explored. For readout, the nuclear spin state is transferred to the electron spin which in turn is converted into a charge state via spin exchange interactions with a nearby readout atom. The charge state is then detected with a single electron transistor.

The Hamiltonian for P in Si is given by [57]:

$$H = \mu_B B \sigma_z^e - g_n \mu_n B \sigma_z^n + A \boldsymbol{\sigma}^e \cdot \boldsymbol{\sigma}^n \qquad (58)$$

where μ_B is the Bohr magneton, μ_n is the nuclear magneton, g_n is the nuclear g-factor, B is the applied magnetic field (assumed parallel to z) and $\boldsymbol{\sigma}$ are the Pauli matrices, with superscripts e and n for electron and nuclear. For two coupled qubits the Hamiltonian becomes:

$$H = H(B) + A_1 \boldsymbol{\sigma}^{1n} \cdot \boldsymbol{\sigma}^{1e} + A_2 \boldsymbol{\sigma}^{2n} \cdot \boldsymbol{\sigma}^{2e} + J \boldsymbol{\sigma}^{1n} \cdot \boldsymbol{\sigma}^{2e} \qquad (59)$$

where $H(B)$ is the magnetic field part and the superscripts 1 and 2 refer to the two spins,

$$4J \cong 1.6 \frac{e^2}{\varepsilon a_B} \left(\frac{r}{a_B} \right)^{5/2} e^{\frac{-2r}{a_B}} \qquad (60)$$

where r is the distance between P atoms, ε is the dielectric constant of silicon, and a_B is the effective Bohr radius.

Many of the more challenging operations proposed for the P in Si quantum computer have recently be demonstrated in quantum wells/dots using individual electrons and/or excitons [100]. In most of these experiments electron spins, rather than nuclear spins, are the qubits. Unfortunately, these experiments are usually done in GaAs which is not a spin-free host and so decoherence is a problem. Spin-free semiconductor hosts exist, but fabrication in these systems is not yet as mature (except for silicon).
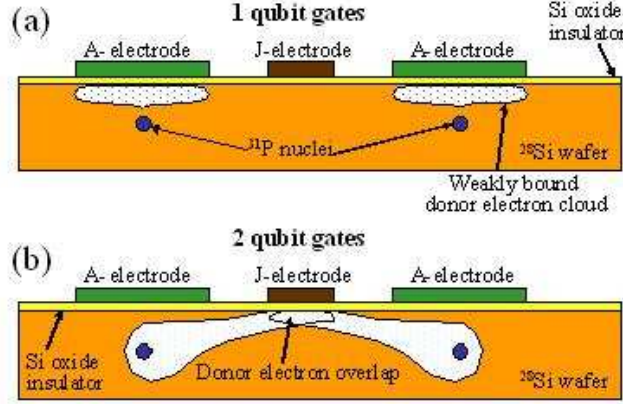
Fig. 12. Operation of the P doped Si quantum computer. (a) Single qubits are tuned into resonance with applied microwave field using voltages on A-electrodes to distort weakly bound electron cloud. (b) Two qubit gates are enabled by using voltages on J-electrodes to overlap neighboring electron clouds, thereby switching on spin exchange coupling.

While the exciting prospect of single electron and/or nuclear spin detection is currently a technical challenge for most solids, it was done long ago in nitrogen-vacancy (NV) diamond [45]. In this optically active SHB material, single electron spin qubits are routinely initialized and read out with high fidelity at liquid helium temperature. In fact, the fidelity is so high that it begins to compare to trapped ions [50]. The electron spin coherence has also been transferred to nearby nuclear spins to perform (non-scalable) two qubit logic [51]. Single qubit logic is usually done with RF pulses, but optical Raman transitions between spin sublevels have been observed in NV diamond under certain experimental conditions [47]. Two qubit gates can be performed using the electron spin coupling between adjacent qubits. Initialization of such a two-qubit system consisting of an NV and nearby N atom has recently been demonstrated using optical pumping. Scalability of this system can be achieved using an electron spin resonance (ESR) version of a Raman transition to transfer this spin coupling to the nuclear spins [111]. This ESR Raman has already been demonstrated for single NV spins.

The spin Hamiltonian for NV diamond is given by [90]:

$$H = D(S_z^2 - \frac{1}{3}S^2) + \beta_e \mathbf{B} \overleftrightarrow{g}_e \mathbf{S} + \mathbf{S} \overleftrightarrow{A} \mathbf{I} + P(I_z^2 - \frac{1}{3}I^2) \tag{61}$$

where D is the zero-field splitting, $\mathbf{B}$ is the applied magnetic field, $\overleftrightarrow{A}$ is the electron-nuclear hyperfine coupling tensor, $\mathbf{S}$ and $\mathbf{I}$ are the electron and nuclear spin vectors, and P is the nuclear quadrupole contribution.

With optical Raman, it should be possible use long-range optical dipole-dipole coupling [77], or eventually cavity-based Quantum ElectroDynamic (QED) coupling, to perform two qubit spin logic, see Fig. 13. If successful, this will be highly scalable because the optical transition frequency can be tuned where desired using dc electric Stark shifts created by gate electrodes (A-electrodes). By requiring both optical laser frequency and electrode voltages to be correctly tuned, qubit excitation becomes very selective and two-qubit coupling only exists when needed, in contrast to the usual case in NMR.
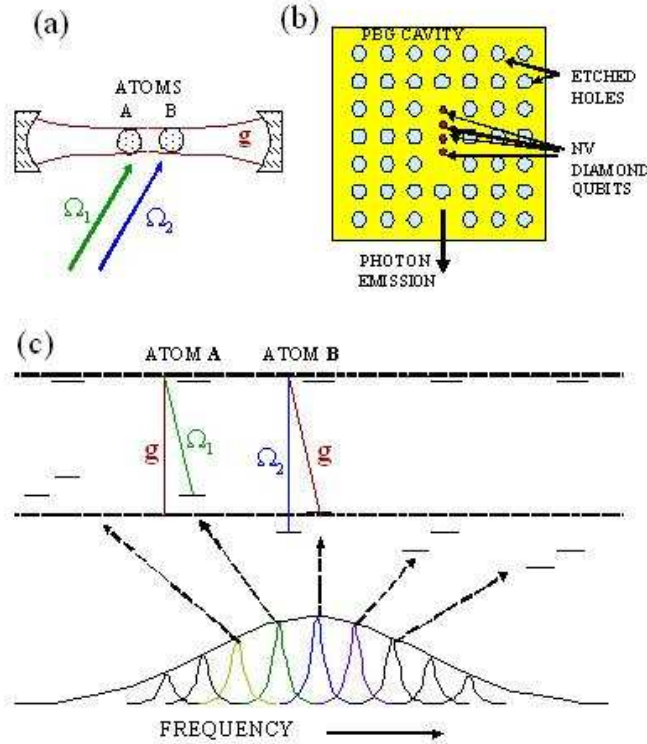
Fig. 13. (a) Two distant qubits coupled by vacuum mode of cavity using cavity QED. (b) Possible implementation of multi-qubit bus using photon band gap cavity in NV diamond. (c) Illustration of the use of optical Raman with cavity QED to couple spectrally adjacent qubits.

Electron spin population lifetimes up to minutes have so far been observed at low temperature, with coherence lifetimes up to 0.3 milliseconds at room temperature [50]. Interestingly, the optical initialization and readout still works at room temperature (though with less fidelity), as well as the ESR Raman transitions. This raises the intriguing question of whether or not

a room-temperature solid-state NMR quantum computer can eventually be built using NV diamond.

4 Shor's algorithm and its experimental realization

Through the rest of the paper, we will describe two applications of the NMR quantum computer: the Shor's algorithm and a lattice algorithm. Shor's algorithm for the factorization of integers aimed at decryption is a special example of a "killer ap" of quantum computing [28, 94]. Recently, a successful experiment has shown the potential capability of the implementation of Shor's algorithm, although it is still very simple and tentative. In [109], Vandersypen et al. factor 15 into 3 times 5. That work has demonstrated the liquid NMR quantum computer to be the most successful quantum computer so far.

4.1 Shor's algorithm

It is not difficult to factor a composite integer (i.e., non-prime) into prime numbers when that integer is small, but the computation burden grows rapidly when the number increases. The currently most efficient algorithm, the number field sieve, requires an exponential running time $e^{c(\log n)^{1/3}(\log\log n)^{2/3}}$, where n is the number to be factored and clearly $\log n$ is proportional to the number of the bits needed to store this number. This makes it practically impossible to factor a large number using a classical computer. This difficulty is used to construct several cryptosystems, such as the RSA public key cryptosystem [93]. Peter W. Shor has shown that this problem can be solved in polynomial running time instead of exponential time by using the quantum computer. A more accessible account of Shor's algorithm is given by Lomonaco [72].

Let n be an odd integer to be factored, and choose another random integer x less than n. We require x to be coprime with n; otherwise, we find a factor of n immediately by the Euclidean method. It is then known that function $f(s) = x^s \mod n$ is periodic. The period of f (and also of x) is the smallest integer r such that $x^r = 1 \mod n$. For example, when $n = 15$ and $x = 3$, the moduli of x^s, with s being 1, 2, 3, ..., are 3, 9, 12, 6, 3, 9, 12, 6, ..., and the period is 4.

Now we check the period r. If r is even, $r = 2t$, then $x^{2t} - 1 = (x^t + 1)(x^t - 1) = 0 \mod n$, so either $x^t - 1$ or $x^t + 1$ has a common factor with n. A classical computer can use the Euclidean algorithm to compute the greatest common divisors, denoted as $\gcd(x^t + 1, n)$ and $\gcd(x^t - 1, n)$, in polynomial time. It is possible that we only obtain the trivial factors 1 or n using the x we choose. This happens only when $x^t = -1 \mod n$, since $x^t - 1 = 0 \mod n$ can not happen with r being already the smallest integer such that $x^r = 1 \mod n$. Fortunately it has been proved that the probability to meet such a bad x is at most $1/2^k$, where k is the number of distinct prime factors of n. Since k is

at least 2, the probability is still large enough for us to find a good x, which has an even period r and $x^t \neq -1 \mod n$.

A quantum computer can find the period r efficiently because of the speedup afforded by quantum Fourier transform (QFT). Let us have two b-qubit registers. We select b large enough such that we can observe many periods. At the beginning, we set the two registers to state $|0\rangle$. Then we randomize the first register to a new state

$$|\psi_1\rangle = \frac{1}{\sqrt{S}} \sum_{k=0}^{S-1} |k\rangle|0\rangle, \tag{62}$$

where $S = 2^b$, the number of the total b-qubit states of the first register, with b large enough such that $2n^2 > S > n^2$.

We now design a certain series of pulses to compute $f(k) = x^k \mod n$, and change the quantum state to

$$|\psi_2\rangle = \frac{1}{\sqrt{S}} \sum_{k=0}^{S-1} |k\rangle|f(k)\rangle. \tag{63}$$

Now, apply QFT [88] to the first register in (63), which is a unitary transform mapping every $|k\rangle$ to another state:

$$|k\rangle \rightarrow \frac{1}{\sqrt{S}} \sum_{k=0}^{S-1} e^{2\pi i u k/S} |u\rangle. \tag{64}$$

Then the quantum state of the system changes to

$$|\psi_3\rangle = \frac{1}{S} \sum_{u=0}^{S-1} |u\rangle \sum_{k=0}^{S-1} e^{2\pi i u k/S} |f(k)\rangle. \tag{65}$$

Assume that $f(k)$ has period r, and we write $k = d+jr$ such that $0 \leq d < r$, where d is the remainder of k after it is divided by r and j ranges from 0 to A, the largest integer such that $Ar < S$. This way, we can write $|\psi_3\rangle$ as

$$|\psi_3\rangle = \frac{1}{S} \sum_{u=0}^{S-1} |u\rangle \sum_{d=0}^{r-1} |f(d)\rangle e^{2\pi i u d/S} \sum_{j=0}^{A} e^{2\pi i u r j/S} I_{(d+rj<S)},$$

where $I_{(d+rj<S)} = 1$ when $d + rj < S$, and 0 otherwise. If $S = (A+1)r$, $I_{(d+rj<S)} = 1$ for every d and j. If $S \neq (A+1)r$, it is still reasonable to ignore the difference and let $I_{(d+rj<S)} = 1$ everywhere because we have chosen S large enough. In this case, we let

$$b_u = \frac{1}{S} \sum_{j=0}^{A} e^{2\pi i u r j/S} = \frac{1}{S} \left(\frac{1 - e^{2\pi i u r(A+1)/S}}{1 - e^{2\pi i u r/S}} \right), \tag{66}$$

thus our quantum state is now

$$|\psi_3\rangle = \frac{1}{S} \sum_{u=0}^{S-1} \sum_{d=0}^{r-1} b_u e^{2\pi i u d/S} |u\rangle |f(d)\rangle.$$

We can now measure the first register, and we want to find such a u, for which there is an l satisfying

$$\left| \frac{u}{S} - \frac{l}{r} \right| \leq \frac{1}{2S}. \tag{67}$$

There are about r such u's, and it has been estimated that the probability to find such a u is at least 0.4 [88]. Because $\frac{1}{2S} < \frac{1}{2n^2}$, and we know that $r < n$, there is at most one fraction $\frac{k}{r}$ satisfying the condition and we can use *continued fraction expansions* to find the fraction. If k and r are coprime, we obtain r as the denominator of the fraction. If not, we only find a factor of r. If r is odd or $x^{r/2}$ does not give us a useful result, choose another x and try again. It may be necessary to try several (of the order $\mathcal{O}(\log\log n)$) times until r is successfully found, but the overall running time is still reasonable.

4.2 Circuit design for Shor's algorithm

Before we introduce the experiment by Vandersypen, et al. [109], we extend the above discussion a little further to the case when r divides S. Now S/r becomes an integer and (66) always holds so that S doesn't have to be very large. Moreover, (67) becomes an identity

$$u = \frac{l \cdot S}{r}, \tag{68}$$

i.e., r is the denominator of the fraction $\frac{u}{S}$ after cancelling the common factor between u and S if l and r are coprime. The integer 15 falls into this situation. The possible x can be 2, 4, 7, 8, 11, or 13. When we choose x to be 2, 7, 8 or 13, the period r is 4. In other cases, r is 2. The period r divides $S = 2^b$ in both cases. Only 2 qubits at most are required to compute one period of f. In the experiment, 3 qubits are used to obtain more periods.

Vandersypen et al. used liquid NMR to realize Shor's algorithm in factorizing 15. The sample in the experiment is a custom-synthesized material whose molecules have five ^{19}F and two ^{13}C, so it has seven qubits ready for use. Those seven qubits are divided into two registers, 3 to store the number k (the first register, represented by $|k_2 k_1 k_0\rangle$) and 4 to store the modular exponentiation y (the second register, represented by $|y_3 y_2 y_1 y_0\rangle$), see Fig. 14 and Fig. 15. The total Hamiltonian is

$$H = \sum_{i=1}^{7} \frac{1}{2} \omega_i \sigma_z^i + \frac{1}{2} \sum_{i<j} J_{ij} \sigma_z^i \sigma_z^j.$$

Each run of the experiment consists of 4 steps. In the first step, the sample is initialized to a certain pseudo-pure state; in the second step, a series of specially designed pulses are applied to realize the computation of modular exponentiation; in the third step, QFT is applied to the first register; finally, the period was obtained through the reading of the spectrum. The system begins from thermal equilibrium, where the density matrix is given by $\rho_0 = e^{-H/kT} \approx I - \frac{H}{kT}$. A suitable initial pseudo-pure state $|\psi_1\rangle = |0000001\rangle$ is obtained by the temporal averaging method.

Although it is difficult to design a general circuit for the modular exponentiation, it is easy to "hard-wire" for this special case in consideration. As the exponent k can be written as $k = k_0 + 2k_1 + 4k_2$, we can change the modular exponential x^k mod 15 into successive operations of modular multiplications by $x^{2^i k_i}$, with $i = 0, 1, 2$, applied to the second register y beginning from $y = 1$.

When $i = 0$, $y \cdot x = x = 1 + (x - 1)$, so the multiplication is actually a controlled-addition with $(x - 1)$ in case $k_0 = 1$. For $x = 7 = (0111)_2$, it is equal to flip the state of y_1 and y_2 ($y = (0001)_2$ before the multiplication). For $x = 11 = (1011)_2$, the same reasoning shows that we only have to flip the state of y_3 and y_1, depending on k_0. Gates A and B in Figs. 14 and 15 accomplish the modular multiplication x^{k_0}.

The situation is a little more complicated for $i = 1$. We only discuss the situation when $k_1 = 1$, since y will not change when $k_1 = 0$. Different strategies are needed for $x = 7$ and $x = 11$. When $x = 11$, since $11^2 = 121 = 15 \times 8 + 1$, $y \times 11^2 = y$ (mod 15). We need to do nothing and the same result holds for the third qubit k_2. When $x = 7$, we can design the circuit by first investigating the following identity

$$
\begin{aligned}
y \cdot 7^2 &= y \cdot 4 \quad \mod 15 \\
&= (y_0 + 2y_1 + 4y_2 + 8y_3) \cdot 4 \quad \mod 15 \\
&= (4y_0 + 8y_1 + 16y_2 + 32y_3) \quad \mod 15 \\
&= (y_2 + 2y_3 + 4y_0 + 8y_1) \quad \mod 15 \\
&= (y_2 \cdot 2^0 + y_3 \cdot 2^1 + y_0 \cdot 2^2 + y_1 \cdot 2^3) \quad \mod 15.
\end{aligned}
$$

It shows that the modular multiplication can be achieved by exchanging the first qubit y_0 with the third qubit y_2, and the second qubit y_1 with the fourth qubit y_3. In Fig. 14, gates C, D, and E are used to accomplish the former, and gates F, G, and H the latter. Further simplification of the circuit can be made. Since the control bit y_3 is $|0\rangle$ before gate C, that gate can just be omitted. Gates H and E have no effect on the period; they can be omitted, too.

The circuit design for the quantum Fourier transform is just a standard design; see, e.g., [28, Fig. 5]. It has 3 Hadamard gates and 3 controlled-phase gates. Figs. 14 and 15 show the circuit designs for $y = 7$ and $y = 11$. Totally about 300 pulses are used in the experiment and it takes about 700ms to accomplish all steps in the case of $x = 7$.
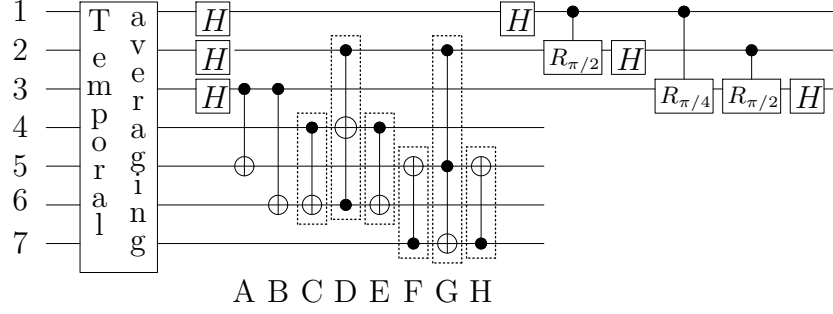
Fig. 14. The quantum circuit for the (hard) case for the realization of Shor's Algorithm ($x = 7$). From top to bottom, the qubits are k_2, k_1, k_0, y_3, y_2, y_1 and y_0, respectively, in sequential order.
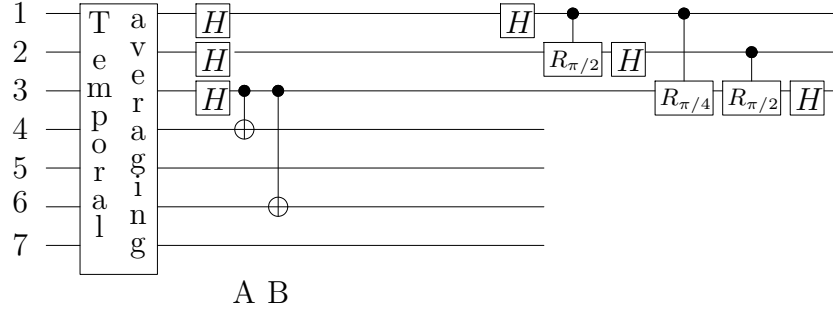
Fig. 15. The quantum circuit for the (easy) case for realization of Shor's Algorithm ($x = 11$). From top to bottom, the qubits are k_2, k_1, k_0, y_3, y_2, y_1 and y_0, respectively, in sequential order.

4.3 Experimental result

Readout of the experiment needs a careful interpretation of the data. Because an NMR sample consists of many molecules, the readout is the average value of u from all molecules instead of the reading from a single molecule.

Both qubits k_0 and k_1 are found to be in state $|0\rangle$ after the extraction of the spectra [109] for the easy case of $x = 11$, while qubit k_2 is in a equally mixture state of $|0\rangle$ and $|1\rangle$. Thus the possible u can be 0 and 4, i.e., 000 and 100 in binary form. From (68), r can be obtained as $r = 8/4 = 2$, and the greatest common divisors are computed as $\gcd(11^{2/2} + 1, 15) = 3$ and $\gcd(11^{2/2} - 1, 15) = 5$.

In the case of $x = 7$, the spectra in [109] indicate that only qubit k_0 is in state $|0\rangle$, and both qubits k_1 and k_2 are in equal mixture of states $|0\rangle$ and $|1\rangle$. Thus u is in a mixture of states $|0\rangle$, $|2\rangle$, $|4\rangle$ and $|6\rangle$. We can see that the period of u is 2, thus the period of the modular exponent r is $8/2 = 4$. The factors of 15 can finally be obtained as $\gcd(7^{4/2} - 1, 15) = 3$ and $\gcd(7^{4/2} + 1, 15) = 5$.

5 Quantum algorithm for lattice-gas systems

In the previous sections, we have explained how to construct a quantum computer using liquid NMR and illustrated a successful experiment. We have taken it for granted that the coherence can be maintained long enough and different qubits can be entangled even if they are separated far apart in space. Unfortunately, these assumptions are not always practical and in fact they constitute great obstacles to overcome. The problem becomes more serious when more qubits are involved. *Type-II quantum computers* are proposed to alleviate this problem. A type-II quantum computer is composed of a network or array of small quantum computers interconnected by classical communication channels [118]. In stead of the global coherence and entanglement, only local coherence and entanglement within every small quantum computer, called a *node*, are required, and the difficulty faced by the centralized quantum computer is dramatically eased.

The wave function of the whole type-II quantum computer system is a tensor product over all the nodes:

$$|\psi(t)\rangle = |\psi(x_1, t)\rangle \otimes \quad \cdots \quad \otimes |\psi(x_N, t)\rangle, \tag{69}$$

where N is the number of nodes. The lattice gas algorithm (LGA) is specially suited for this structure. Every computation cycle can be broken up into three steps with two intermediate states $|\psi'\rangle$ and $|\psi''\rangle$:

$$\begin{aligned} |\psi'\rangle &= \hat{C}|\psi(t)\rangle, \\ |\psi''\rangle &= \Gamma|\psi'\rangle, \\ |\psi(t+1)\rangle &= T|\psi''\rangle, \end{aligned} \tag{70}$$

where $\hat{C}$ is a unitary operator acting locally on every node, while Γ is a projection operator, such as a measurement, and T is the streaming operator which exchanges information among nodes. The type-II quantum computer takes advantage of parallelism in two ways: one classical, all the nodes work simultaneously; the other quantum, quantum entanglement is still kept inside every node. Because measurement is applied and the system is reset at the end of every computation cycle, the coherence only needs to be maintained for a short time.

5.1 Quantum algorithm for a lattice-gas model

Consider a one-dimensional diffusion equation without boundary condition

$$\frac{\partial \rho}{\partial t} = \frac{\partial^2 \rho}{\partial x^2}, \tag{71}$$

where ρ is the mass density or temperature function along the x-axis. Using the finite difference method, we can write a finite difference approximation to solve the above partial differential equation numerically:

$$\frac{\rho(x, t+\tau) - \rho(x, t)}{\tau} = \frac{\rho(x+l, t) - 2\rho(x, t) + \rho(x-l, t)}{l^2}, \tag{72}$$

where τ is the time step size and l is the space step size. From physics, we know that the above equation may be studied by a lattice gas algorithm. Without loss of generality, we assume that τ and l are normalized so that the difference equation can be written as

$$\rho(x_i, k+1) - \rho(x_i, k) = \frac{1}{2}(\rho(x_{i+1}, k) - 2\rho(x_i, k) + \rho(x_{i-1}, k)).$$

Points x_i are evenly distributed along the x-axis, also called *nodes*. To study the above equation, two functions, $f_1(x_i, k)$ and $f_2(x_i, k)$, called *channels*, are defined for each node x_i at time k. The set of values of these two functions is called the *state* of node x_i. Any physical observable, such as the density function $\rho(x_i, k)$, is a function of the state at the node. The evolution of the lattice, or the state of all nodes, consists of two operations: *collision* and *propagation*. A collision is a local operator only defined by the state of the node itself. The propagation operator transfers information from one node to another and the state at one node changes according to the state of other nodes. This is completed by defining a velocity vector for every channel which gives the information flow a direction. In our special example here, information in the two channels flows in opposite directions. After propagation, one channel gets its new value from its left neighbor, while the other from its right neighbor. This LGA is completed with a Type II quantum computer by J. Yepez of the Air Force Research Laboratory and M.A. Pravia, et al. of the Department of Nuclear Engineering at MIT [7, 91, 117, 118]. The actual result is not as good as desired, but improvement is still possible.

To store a floating point number, a classical computer uses a register with 32 or 64 bits, depending on the machine. Quantum computers presently have difficulty to do it the same way as classical computers because there is not yet the technology for 32 or 64 qubits. In this quantum lattice-gas algorithm, a two qubit system is proposed for every node. The two qubits are represented by $|q_1(x_i, k)\rangle$ and $|q_2(x_i, k)\rangle$, respectively, and

$$|q_1(x_i, k)\rangle = \sqrt{f_1(x_i, k)}|0\rangle + \sqrt{1 - f_1(x_i, k)}|1\rangle,$$

$$|q_2(x_i, k)\rangle = \sqrt{f_2(x_i, k)}|0\rangle + \sqrt{1 - f_2(x_i, k)}|1\rangle.$$

The state of the whole system $|\psi(x_i, k)\rangle$ at node x_i and time k is a tensor product:

$$\begin{aligned}|\psi(x_i, k)\rangle &= |q_1(x_i, k)\rangle|q_2(x_i, k)\rangle \\ &= \sqrt{f_1(x_i, k)f_2(x_i, k)}|00\rangle + \sqrt{(1 - f_1(x_i, k))f_2(x_i, k)}|10\rangle \\ &+ \sqrt{f_1(x_i, k)(1 - f_2(x_i, k))}|01\rangle \\ &+ \sqrt{(1 - f_1(x_i, k))(1 - f_2(x_i, k))}|11\rangle.\end{aligned}$$

Quantities $f_1(x_i, k)$ and $f_2(x_i, k)$ are the probabilities of occurrence of the state $|0\rangle$ for qubit 1 and 2, respectively, corresponding to the two channels, and

$1 - f_{1,2}(x_i, k)$ are the occurrence probabilities of the state $|1\rangle$. Since the states are normalized, $0 \le f_{1,2}(x_i, k) \le 1$, and we let $\rho(x_i, k) = f_1(x_i, k) + f_2(x_i, k)$. It is noted that our Type-II quantum computer assigns ρ a continuous value (a function of the occurrence probabilities) rather than a discrete value as a digital computer does. An array of two qubit systems are used in the computation, corresponding to a series of nodes.

The quantum LGA here has three steps in every cycle that complete a step of the finite difference algorithm computation: *collision*, *measurement*, and *re-initialization*. The last two composed are equal to one propagation operation in a normal lattice gas algorithm. Because the propagation needs information exchange among different nodes, measurement and classical communication are needed to accomplish one operation. We map the quantum state to a vector in $\mathbf{C}^4$ as that given in (29).

In the collision step, a unitary operator is applied simultaneously to all nodes:

$$|\overline{\psi}(x_i, k)\rangle = U|\psi(x_i, k)\rangle,$$

where

$$U = \begin{bmatrix} 1 & 0 & 0 & 0 \\ 0 & \frac{1}{2} - \frac{i}{2} & \frac{1}{2} + \frac{i}{2} & 0 \\ 0 & \frac{1}{2} + \frac{i}{2} & \frac{1}{2} - \frac{i}{2} & 0 \\ 0 & 0 & 0 & 1 \end{bmatrix}. \tag{73}$$

The new occurrence probabilities of the sate $|0\rangle$ of the two qubits after the operation, $\overline{f}_1$ and $\overline{f}_2$, can be computed using

$$\overline{f}_1 = \langle\overline{\psi}|n_1|\overline{\psi}\rangle, \quad n_1 = \begin{bmatrix} 1 & 0 & 0 & 0 \\ 0 & 1 & 0 & 0 \\ 0 & 0 & 0 & 0 \\ 0 & 0 & 0 & 0 \end{bmatrix},$$

$$\overline{f}_2 = \langle\overline{\psi}|n_2|\overline{\psi}\rangle, \quad n_2 = \begin{bmatrix} 1 & 0 & 0 & 0 \\ 0 & 0 & 0 & 0 \\ 0 & 0 & 1 & 0 \\ 0 & 0 & 0 & 0 \end{bmatrix}, \tag{74}$$

leading to

$$\overline{f}_1(x_i, k) = \tfrac{1}{2}(f_1(x_i, k) + f_2(x_i, k)),$$
$$\overline{f}_2(x_i, k) = \tfrac{1}{2}(f_1(x_i, k) + f_2(x_i, k)).$$

The collision operator is actually doing a job of averaging. The state after the collision is also called the local equilibrium.

In the second step, a measurement is applied at every node and $\overline{f}_{1,2}(x_i, k)$ of all the nodes are retrieved for future use.

In the third step, using information from the measurement from the previous step, the state of all the nodes are re-initialized to a separable state

$$|q_1(x_i, k+1)\rangle = \sqrt{\overline{f}_1(x_{i+1}, k)}|0\rangle + \sqrt{1 - \overline{f}_1(x_{i+1}, k)}|1\rangle,$$
$$|q_2(x_i, k+1)\rangle = \sqrt{\overline{f}_2(x_{i-1}, k)}|0\rangle + \sqrt{1 - \overline{f}_2(x_{i-1}, k)}|1\rangle. \tag{75}$$

It can be seen that the second and third steps have accomplished the propagation operation. At node x_i, the new state of channel one is acquired from the same channel of its right neighbor node x_{i+1}, and channel two acquires its state from its left neighbor. It is complicated here only because the communication between two quantum systems is difficult.

To see how this LGA works, let us begin from a local equilibrium state, $f_1(x_i, k) = f_2(x_i, k) = \rho(x_i, k)/2$, where the states come off a collision operation (step 2). We list the $f_{1,2}$ around position x_i before the third step in two rows

$$f_1 : \quad \ldots \quad \frac{\rho(x_{i-2},k)}{2} \quad \frac{\rho(x_{i-1},k)}{2} \quad \frac{\rho(x_i,k)}{2} \quad \frac{\rho(x_{i+1},k)}{2} \quad \ldots$$
$$f_2 : \quad \ldots \quad \frac{\rho(x_{i-2},k)}{2} \quad \frac{\rho(x_{i-1},k)}{2} \quad \frac{\rho(x_i,k)}{2} \quad \frac{\rho(x_{i+1},k)}{2} \quad \ldots$$

and after the third step

$$f_1 : \quad \ldots \quad \frac{\rho(x_{i-1},k)}{2} \quad \frac{\rho(x_i,k)}{2} \quad \frac{\rho(x_{i+1},k)}{2} \quad \frac{\rho(x_{i+2},k)}{2} \quad \ldots$$
$$f_2 : \quad \ldots \quad \frac{\rho(x_{i-3},k)}{2} \quad \frac{\rho(x_{i-2},k)}{2} \quad \frac{\rho(x_{i-1},k)}{2} \quad \frac{\rho(x_i,k)}{2} \quad \ldots$$

We can see that the row of f_1 (channel one) moves left and the row of f_2 (channel two) moves right. According to our definition, the new value of ρ is the sum of $f_1(x_i, k+1)$ and $f_2(x_i, k+1)$, i.e., $\rho(x_i, k+1) = \frac{1}{2}(\rho(x_{i+1}, k) + \rho(x_{i-1}, k))$. It is easy to check that

$$\rho(x_i, k+1) - \rho(x_i, k) = \frac{1}{2}(\rho(x_{i+1}, k) - 2\rho(x_i, k) + \rho(x_{i-1}, k)),$$

as desired.

Applications of the Type-II quantum computer with quantum LGA also have been reported in the simulation of the time-dependent evolution of a many-body quantum mechanical system [119], solution of a one-dimensional magnetohydrodynamic turbulence [103], representation of solitons [102] and other equations.

5.2 Physical realization and result

The experiment in Subsection 5.1 uses a two-qubit molecule, chloroform, whose structure is shown in Fig. 6. The hydrogen and carbon nuclei serve as qubit 1 and 2, respectively.

The actual results obtained from the experiment are compared with simulation results [91]. After 12 steps, the error becomes very large. Imperfection in the decoupling sequences is blamed and it is believed that the problem can be mitigated when the technology is improved in the future. Extreme requirement of high accuracy in the control pulse and readout is a disadvantage of this Type-II quantum computer, because it uses a continuous representation (the probability of occurrence) instead of a discrete one. Thus, it is more vulnerable to the inaccuracy in the NMR operation. Small errors in every step accumulate and finally become intolerable. Repeated measurement and re-initialization ease the requirement for coherence time, but place a high requirement on the fidelity at the same time.

6 Conclusion

In this article, we present the basic technology used to construct a quantum computer with liquid state NMR. The successful experiments for many algorithms have shown that liquid state NMR is capable of simulating a quantum computer and forms a test bed for quantum algorithms. It is so far the only technology available to realize a 7 qubit algorithm in laboratory. One reason for its success is the robustness of the spin system which only interacts with the external magnetic field, and it is possible to maintain the coherence for a long time (from seconds to hours). Besides, over the 60 years history of NMR spectroscopy, analytic tools have been developed for the purpose of chemical and medical applications, and exact description and dedicated coherence control of the dynamics of the quantum spin system is now available to achieve high accuracy in the pulse design and application. In fact, the experimental techniques established in NMR, especially the coherence control technology, can be easily transferred to other quantum systems if they have a similar Hamiltonian, and the research in NMR is therefor helpful for the development of other more complicated and powerful quantum computers.

Liquid NMR has played a pioneering role in the quantum computer technology development. But its lack of scalability has constitute a severe obstacle to its future applicability. However, in Section 3 we show new technology of *solid state NMR* which has the potential to overcome liquid NMR's difficulties. For solid state NMR, under low temperature, the relaxation times of spins are typically very long, and the coupling between qubits is strong so that the control can be fast and easy. The small ratio of the gate time and the decoherence time makes more gates available, and more complicated algorithms can be tested. The nuclei can be cooled down easily and the spin system is highly polarized. The signal is much stronger so that fewer nuclei are needed. Even without the help of gradient field and the silicon technology, as we have mentioned, a quantum computer with 30 to 40 qubits is envisioned with designed molecules similar to that of the liquid state NMR computer except that the ensemble is in a solid crystal state. This is already a quantum system that reaches the limit a classical computer can simulate. Although it is still not scalable and not a standard quantum computer, these small and medium scale quantum computers will help in the building of a scalable and working quantum computer.

Acknowledgement

7 Appendix

A The Homomorphism from SU(2) to SO(3)

We use the same notation as in Section 2.3. Recall that U is a complex matrix in $\mathbf{SU}(2)$, and we want to find a mapping R from $\mathbf{SU}(2)$ to the space of 3×3 real matrices, so that $R(U)$ and U represent the same physical operation. Let $\mathbf{v}$ be a Bloch vector corresponding to the old state $|\phi\rangle$ and $\mathbf{v}'$ to the new one. Then the following identity must be satisfied:

$$\mathbf{v}' = R(U)\mathbf{v}, \tag{76}$$

where $U \in \mathbf{SU}(2)$. Using the definition of Bloch vector and density matrix, we obtain

$$\begin{aligned}\mathbf{v}' \cdot \mathbf{A} &= U|\psi\rangle\langle\psi|U^\dagger - I_0 \\ &= U\mathbf{v} \cdot \mathbf{A}U^\dagger,\end{aligned} \tag{77}$$

where $\mathbf{A} = [I_x, I_y, I_z]$ and we use the dot to denote the inner product between vectors.

The product of I_i and σ_j satisfies

$$Tr(I_i\sigma_j) = \delta_{ij}, \qquad i, j \in \{x, y, z\},$$

where σ_j are the Pauli matrices. By multiplying both sides of (77) with σ_k and taking the trace of both sides, we obtain

$$\begin{aligned}v'_k &= Tr(\mathbf{v}' \cdot \mathbf{A}\sigma_k) \\ &= Tr(\sigma_k\,U\,I_i\,U^\dagger)v_i,\end{aligned} \tag{78}$$

where v'_k and v_i are, respectively, the k-th an i-th entry of the corresponding vectors. We apply the summation convention in this section, where summing over repeated indices is implied unless otherwise stated. Comparing the above result with equation

$$v'_k = R(U)_{ki}v_i,$$

we obtain the desirable matrix $R(U)$:

$$R(U)_{ki} = Tr(\sigma_k\,U\,I_i\,U^\dagger). \tag{79}$$

Thus we have constructed a mapping from $\mathbf{SU}(2)$ to the set of 3×3 matrices. Let us now tentatively accept the fact the target matrix is real which we will prove later. We first show that $R(U)$ is in fact a proper rotation matrix, i.e., $R(U) \in \mathbf{SO}(3)$ by proving that it is isometric and preserves the three-fold product; cf. (82).

Let $\mathbf{v} = [a \quad b \quad c]^T \in R^3$. First note that we can find its norm by computing the determinant of a special matrix:

$$\det(\mathbf{v} \cdot \mathbf{A}) = \tfrac{1}{4} \begin{vmatrix} c & a - bi \\ a + bi & -c \end{vmatrix}$$
$$= -\tfrac{1}{4}(c^2 + a^2 + b^2) \qquad (80)$$
$$= -\tfrac{1}{4}\|\mathbf{v}\|^2.$$

Together with (77), we see that the transformation is isometric:

$$\|\mathbf{v}'\|^2 = -4\det(\mathbf{v}' \cdot \mathbf{A})$$
$$= -4\det(U\,\mathbf{v} \cdot \mathbf{A}U^\dagger)$$
$$= -4\det(\mathbf{v} \cdot \mathbf{A}) \qquad (81)$$
$$= \|\mathbf{v}\|^2.$$

Direct computation also shows the preservation of the three-fold product, as follows. Let $\mathbf{v}^l$, $l = 1,2,3$ be three vectors on the Bloch sphere, $\mathbf{v}'^l = R(u)\mathbf{v}^l$. We have

$$Tr\left((\mathbf{v}^1 \cdot \mathbf{A})(\mathbf{v}^2 \cdot \mathbf{A})(\mathbf{v}^3 \cdot \mathbf{A})\right) = Tr(v_i^1 v_j^2 v_k^3 I_i I_j I_k)$$
$$= \tfrac{i}{4} v_i^1 v_j^2 v_k^3 \epsilon_{ijk} \qquad (82)$$
$$= \tfrac{i}{4} \mathbf{v}^1 \cdot (\mathbf{v}^2 \times \mathbf{v}^3).$$

The above identity can be used to show the preservation of the *three-fold product*:

$$\mathbf{v}'^1 \cdot (\mathbf{v}'^2 \times \mathbf{v}'^3) = \tfrac{4}{i}Tr\left((\mathbf{v}'^1 \cdot \mathbf{A})(\mathbf{v}'^2 \cdot \mathbf{A})(\mathbf{v}'^3 \cdot \mathbf{A})\right)$$
$$= \tfrac{4}{i}Tr\left((U\mathbf{v}^1 \cdot \mathbf{A}U^\dagger)(U\mathbf{v}^2 \cdot \mathbf{A}U^\dagger)(U\mathbf{v}^3 \cdot \mathbf{A}U^\dagger)\right)$$
$$= \tfrac{4}{i}Tr\left((\mathbf{v}^1 \cdot \mathbf{A})(\mathbf{v}^2 \cdot \mathbf{A})(\mathbf{v}^3 \cdot \mathbf{A})\right) \qquad (83)$$
$$= \mathbf{v}^1 \cdot (\mathbf{v}^2 \times \mathbf{v}^3),$$

and we see that $R(U) \in \mathbf{SO}(3)$. To prove that the mapping is surjective, we introduce a parameterization of $\mathbf{SU}(2)$ in some exponential form. For any $U \in \mathbf{SU}(2)$, we can find a $\theta \in [0, 2\pi)$ and a unit vector $\mathbf{n} \in \mathbf{R}^3$ such that

$$U(\theta, \mathbf{n}) = e^{-i\frac{\theta}{2}\mathbf{n}\cdot\boldsymbol{\sigma}}$$
$$= \begin{bmatrix} \cos\frac{\theta}{2} - in_3\sin\frac{\theta}{2} & -\sin\frac{\theta}{2}(n_2 + in_1) \\ \sin\frac{\theta}{2}(n_2 - in_1) & \cos\frac{\theta}{2} + in_3\sin\frac{\theta}{2} \end{bmatrix} \qquad (84)$$
$$= \cos\frac{\theta}{2}I - i\sin\frac{\theta}{2}\mathbf{n}\cdot\boldsymbol{\sigma},$$

where $\boldsymbol{\sigma} = [\sigma_x, \sigma_y, \sigma_z]$. Every combination of θ and $\mathbf{n}$ also corresponds to a complex matrix in $\mathbf{SU}(2)$. By using (8) and the equality $U(\theta, \mathbf{n})^{-1} = U(\theta, -\mathbf{n})$, the element of $R(U)$ can be computed as

$$R(U)_{ij} = Tr(\sigma_i U I_j U^\dagger)$$
$$= Tr\left(\sigma_i(\cos\frac{\theta}{2}I - i\sin\frac{\theta}{2}\mathbf{n}\cdot\boldsymbol{\sigma})I_j(\cos\frac{\theta}{2}I + i\sin\frac{\theta}{2}\mathbf{n}\cdot\boldsymbol{\sigma})\right)$$
$$= Tr(\sigma_i I_j \cos^2\frac{\theta}{2} + i\sigma_i I_j \mathbf{n}\cdot\boldsymbol{\sigma}\sin\frac{\theta}{2}\cos\frac{\theta}{2} \qquad (85)$$
$$\quad -i\sigma_i\mathbf{n}\cdot\boldsymbol{\sigma}I_j\sin\frac{\theta}{2}\cos\frac{\theta}{2} + \sigma_i\mathbf{n}\cdot\boldsymbol{\sigma}I_j\mathbf{n}\cdot\boldsymbol{\sigma}\sin^2\frac{\theta}{2}).$$

We divide the trace into four parts and compute them separately:

$$Tr(\sigma_i I_j) = \delta_{ij}, \quad Tr(\sigma_i I_j \mathbf{n} \cdot \boldsymbol{\sigma}) = i\epsilon_{ijk} n_k, \quad Tr(\sigma_i \mathbf{n} \cdot \boldsymbol{\sigma} I_j) = i\epsilon_{ikj} n_k, \quad (86)$$

$$Tr(\sigma_i \mathbf{n} \cdot \boldsymbol{\sigma} I_j \mathbf{n} \cdot \boldsymbol{\sigma}) = Tr(\sigma_i \sigma_k I_j \sigma_l n_k n_l)$$

$$= \frac{1}{2} Tr\left((\delta_{ik} I + i\epsilon_{ikm}\sigma_m)(\delta_{jl} I + i\epsilon_{jln}\sigma_n) n_k n_l\right)$$

$$= \delta_{ik}\delta_{jl} n_k n_l - \epsilon_{ikm}\epsilon_{jlm} n_k n_l$$

$$= \delta_{ij} n_i n_j + (2 - \delta_{ij}) n_i n_j - \delta_{ij} = 2 n_i n_j - \delta_{ij}. \quad (87)$$

Substituting (87) and (86) back into (85), we obtain

$$\begin{aligned} R(U)_{ij} &= \cos^2 \tfrac{\theta}{2} \delta_{ij} + \sin^2 \tfrac{\theta}{2} (2 n_i n_j - \delta_{ij}) \\ &\quad - \epsilon_{ijk} n_k \sin \tfrac{\theta}{2} \cos \tfrac{\theta}{2} + \epsilon_{ikj} n_k \sin \tfrac{\theta}{2} \cos \tfrac{\theta}{2} \\ &= \cos\theta \, \delta_{ij} + (1 - \cos\theta) n_i n_j + \sin\theta \, \epsilon_{ikj} n_k, \end{aligned} \quad (88)$$

showing that $R(U)_{ij}$ is *real*. We also claim that $R(U)$ is a rotation about the axis $\mathbf{n}$ with angle θ in the three dimensional Euclidean space by comparing it with the standard formula of a rotation matrix. Because every matrix in $\mathbf{SO}(3)$ can be regarded as a rotation about a certain axis with a certain angle, that matrix is now shown to be an image of some $U \in \mathbf{SU}(2)$. Thus the mapping is surjective.

Finally, we want to show that this mapping from $\mathbf{SU}(2)$ to $\mathbf{SO}(3)$ is a homomorphism and to investigate the multiplicity. Let U and T be two matrices in $\mathbf{SU}(2)$, $\mathbf{v}$ be an arbitrary vector on the Bloch sphere, and $\mathbf{v}' = R(U)\mathbf{v}$, $\mathbf{v}'' = R(T)\mathbf{v}' = R(T)R(U)\mathbf{v}$. Using (77) repeatedly, we obtain

$$\mathbf{v}'' \cdot \mathbf{A} = T(\mathbf{v}' \cdot \mathbf{A})T^\dagger = TU(\mathbf{v} \cdot \mathbf{A})U^\dagger T^\dagger = R(TU)\mathbf{v} \cdot \mathbf{A},$$

thus $\mathbf{v}'' = R(TU)\mathbf{v}$. Because $\mathbf{v}$ is arbitrary, $R(VU) = R(V)R(U)$, implying that the mapping is a homomorphism.

For the multiplicity of this mapping, we investigate the kernel of R, $ker(R)$, which is an invariant subgroup of $\mathbf{SU}(2)$, and the quotient group $\mathbf{SU}(2)/ker(R)$ will then be isomorphic to $\mathbf{SO}(3)$. Suppose that $U \in \mathbf{SU}(2)$ and $R(U) = I_3$, the identity matrix in $\mathbf{SO}(3)$. Then for any $\mathbf{v}$ on the Bloch sphere or R^3, we have equality $\mathbf{v} \cdot \mathbf{A} = U(\mathbf{v} \cdot \mathbf{A})U^\dagger$, since $\mathbf{v} = I\mathbf{v}$. Multiplying both sides with U from the right and using (84), we have

$$\mathbf{v} \cdot \mathbf{A}(\cos \frac{\theta}{2} I - i \sin \frac{\theta}{2} \mathbf{n} \cdot \boldsymbol{\sigma}) = (\cos \frac{\theta}{2} I - i \sin \frac{\theta}{2} \mathbf{n} \cdot \boldsymbol{\sigma})\mathbf{v} \cdot \mathbf{A}.$$

Subtract from both sides the term $\mathbf{v} \cdot \mathbf{A} \cos \frac{\theta}{2} I$,

$$(\mathbf{v} \cdot \mathbf{A}) (\mathbf{n} \cdot \boldsymbol{\sigma}) \sin \frac{\theta}{2} = (\mathbf{n} \cdot \boldsymbol{\sigma}) (\mathbf{v} \cdot \mathbf{A}) \sin \frac{\theta}{2}.$$

Assuming that $\sin \frac{\theta}{2} \neq 0$, we can divide this factor from both sides to obtain

$$(\mathbf{v} \cdot \mathbf{A}) (\mathbf{n} \cdot \boldsymbol{\sigma}) = (\mathbf{n} \cdot \mathbf{A}) (\mathbf{v} \cdot \boldsymbol{\sigma}).$$

Let $\mathbf{v} = [1, 0, 0]^T$. Using properties of Pauli matrices, we obtain

$$n_2 I_z - n_3 I_y = 0.$$

The above is possible only when $n_2 = n_3 = 0$. Trying other different $\mathbf{v}$ leads to $n_1 = 0$, too. This is a contradiction, because we know that $\mathbf{n}$ is a unit vector. Thus we need $\sin\frac{\theta}{2} = 0$. In this case $U = I$ or $U = -I$ and it is easy to verify that these two are really mapped to the identity in $\mathbf{SO}(3)$. Now, we can conclude that the mapping we defined by (79) is a *two-to-one homomorphism* from $\mathbf{SU}(2)$ to $\mathbf{SO}(3)$ with kernel $ker(R) = \{I, -I\}$. The mapping is also surjective, so it defines an isomorphism from the quotient group $\mathbf{SU}(2)/ker(R)$ to $\mathbf{SO}(3)$. The two elements in the kernel, $\pm I$, are in fact the same transformation for quantum systems because only the relative phase matters for a quantum system. For any $O \in \mathbf{SO}(3)$, the two elements in $R^{-1}(O)$, U and $-U$ for some $U \in \mathbf{SU}(2)$, represent the same transformation, too. Thus, nothing is lost if we employ $\mathbf{SO}(3)$ to represent the transformations of a one-spin quantum system.

References

1. E. Abe, K.M. Itoh, T.D. Ladd, J.R. Goldman, F. Yamaguchi, and Y. Yamamoto, Solid-state silicon NMR quantum computer, *Journal of Superconductivity: Incorporating Novel Magnetism* **16**(2003), 1, 175–178.
2. A. Barenco, C.H. Bennett, R. Cleve, D.P. DiVincenzo, N. Margolus, P. Shor, T. Sleator, J. Smolin, and H. Weinfurter, Elementary gates for quantum computation, *quant-ph*/9503016.
3. S. Bartlett, *http://www.physics.usyd.edu.au/ bartlett/ISIT2005/.*
4. P. Benioff, The computer as a physical system: A microscopic quantum mechanical Hamiltonian model of computers as represented by Turing machines, *J. Stat. Phys.* **22** (1980), 563-591.
5. C.H. Bennett, G. Brassard, C. Crepeau,, R. Jozsa, A. Peres, and W. Wootters, Teleporting an unknown quantum state via dual classical and EPR channels, *Phys. Rev. Lett.* **70**(1993), 1895-1899.
6. C.H. Bennett, and P. Shor, Quantum information theory, *IEEE Transaction on Information Theory* **44**(1998), 2724-2742.
7. G.P. Berman, A.A. Ezhov, D.I. Kamenev, and J. Yepez, Simulation of the diffusion equation on a type-II quantum computer, *Phys. Rev. A* **66**(2002), 012310.
8. E. Bernstein and U. Vazirani, Quantum complexity theory, *SIAM J. Comput.* **26**(1997), 1411-1473.
9. F. Bloch, Nuclear induction, *Phys. Rev.* **70**(1946), 460–474.
10. D. Bouwmeester, J.W. Pan, K. Mattle, M. Eibl, H. Weinfurter, and A. Zeilinger, Experimental quantum teleportation, *Nature* **390**(1997), 575-579.
11. G. Burkard, D. Loss and D. DiVincenzo, Coupled quantum dots as quantum gates, Phys. Rev. B **59** (1999), 2070-2078.
12. A.M. Childs, I.L. Chuang, and D.W. Leung, Realization of quantum process tomography in NMR, *Phys. Rev. A* **64**(2001), 012314.

13. I.L. Chuang, L.M.K. Vandersypen, X. Zhou, D.W. Leung, and S. Lloyd, Experimental realization of a quantum algorithm, *Nature* **393**(1998), 143–146.

14. I.L. Chuang, Quantum computation with nuclear magnetic resonance, in *Introduction to Quantum Computation and Information*, edited by H. Lo, S. Popescu, and T. Spiller, World Scientific, Singapore, 1998.

15. I.L. Chuang, and Y. Yamamoto, Simple quantum computer, *Phys. Rev. A* **52**(1995), 5, 3489–3496.

16. D.G. Cory, M.D. Price, and T.F. Havel, Nuclear magnetic resonance spectroscopy: An experimentally accessible paradigm for quantum computing, *Physica D* **120**(1998), 82–101.

17. D.G. Cory, A.F. Fahmy, and T.F. Havel, Ensemble quantum computing by NMR spectroscopy, *Proc. Natl. Acad. Sci. USA* **94**(1997), 1634–1639.

18. D.G. Cory, R. Laflamme, and E. Knill et al., NMR based quantum information processing: achievement and prospect, *Fortschr. Phys.* **48**(2000), 875 – 907.

19. H.K. Cummings, and J.A. Jones, Use of composite rotations to correct systematic errors in NMR quantum computation, *New Journal of Physics* **2**(2000) 6.1 – 6.12.

20. D. Deutsch, Quantum theory, the Church-Turing Principle and the universal quantum computer, *Proc. R. Soc. Lond. A* **400**(1985), 97.

21. D. Deutsch, Quantum computational networks, *Proc. R. Soc. London A* **425**(1989), 73.

22. D. Deutsch and R. Jozsa, Rapid solution of problems by quantum computer, *Proc. R. Soc. London. A* **439**(1992), 553–558.

23. D.P. DiVincenzo, Two-bit quantum gates are universal for quantum computation, *Phys. Rev. A* **51**(1995), 1015–1022.

24. K. Dorai, and D. Suter, Efficient implementations of the quantum Fourier transform: an experimental perspective, *International Journal of Quantum Information* **3**(2005), 2, 413–424.

25. K. Dorai, Arvind, and A. Kumar, Implementing quantum-logic operations, pseudopure states, and the Deutsh-Jozsa algorithm using noncommuting selective pulses in NMR, *Phys. Rev. A* **61**(2000), 042306.

26. J.C. Edwards, *http://www.process-nmr.com/nmr.htm*

27. A. Ekert, Quantum cryptography based on Bell's Theorem, *Phys. Rev. Lett.* **67**(1991), 661-663.

28. A. Ekert and R. Jozsa, Quantum computation and Shor's factoring algorithm, *Reviews of Modern Physics* **68**(1996), 3, 733–753.

29. J.W. Emsley, J. Feeney and L.H. Sutcliffe, *High Resolution Nuclear Magnetic Resonance Spectroscopy*, Pergamon Press, Oxford, 1965.

30. R.W. Equall, Y. Sun, and R.M. Macfarlane, Ultraslow Optical Dephasing In Eu-3+-Y2SiO5, *Phys. Rev. Lett.* **72**(1994), 2179–2181.

31. X. Fang, X. Zhu, M. Feng, X. Mao, and F. Du, Experimental implementation of dense coding using nuclear magnetic resonance, *Phys. Rev. A* **61**(2000), 022307.

32. S. Fernbach, and W.G. Proctor, Spin-echo memory device, *J. of Applied Physics* **26**(1955), 2, 170–181.

33. R.P. Feynman, Simulating physics with computers, *Int. J. Theor. Phys.* **21**(1982), 467.

34. E.M. Fortunato, M.A. Pravia, N. Boulant, et al., Design of strongly modulating pulses to implement precise effective Hamiltonians for quantum information processing, *J. of Chemical Physics* **116**(2002), Issue 17, 7599–7606.

35. E. Fraval, M.J. Sellars, and J.J. Longdell, Dynamic decoherence control of a solid-state nuclear-quadrupole qubit, *Phys. Rev. Lett.* **95**(2005), 030506.

36. E. Fraval, M.J. Sellars, and J.J. Longdell, Method of extending hyperfine coherence times in Pr3+: Y2SiO5, *Phys. Rev. Lett.* **92**(2004), 077601.

37. R. Freeman, Shaped radiofrequency pulses in high resolution NMR, *J. of Progress in Nuclear Magnetic Resonance Spectroscopy* **32**(1998), 59 – 106.

38. C.A. Fuchs, Distinguishability and accessible information in quantum theory, Ph.D. Dissertation, University of New Mexico; *quant-ph*/9601020.

39. B. Fung, and V.L. Ermakov, A simple method for the preparation of pseudopure states in nuclear magnetic resonance quantum information processing, *Journal of Chemical Physics* **121**(2004), 17, 8410 – 8414.

40. N. Gershenfeld, and I.L. Chuang, Bulk spin-resonance quantum computation, *Science* **275**(1997), 350–356.

41. S.J. Glaser, T. Schulte-Herbruggen, M. Sieveking, O. Schedletzky, N.C. Nielsen, O.W. Sorensen, and C. Griesinger, Unitary control in quantum ensembles: maximizing signal intensity in coherent spectroscopy, *Science* **280**(1998), Issue 5362, 421–424.

42. D. Gottesman, and I.L. Chuang, Demonstrating the viability of universal quantum computation using teleportation and single-qubit operations, *Nature* **402**(1999), 390–393.

43. J.R. Goldman, T.D. Ladd, F. Yamaguchi, and Y. Yamamoto, Magnet designs for a crystal-lattice quantum computer, *Appl. Phys. A* **71**(2000), 11–17.

44. L.G. Grover, Quantum mechanics helps in searching for a needle in a haystack, *Phys. Rev. Lett.* **79**(1997), 325.

45. A. Gruber, A. Drabenstedt, C. Tietz, L. Fleury, J. Wrachtrup, and C. von-Borczyskowski, Scanning confocal optical microscopy and magnetic resonance on single defect centers, *Science* **276**(1997), Issue 5321, 2012–2014.

46. P.C. Hansen, M.J.M. Leask, B.M. Wanklyn, Y. Sun, R.L. Cone, and M.M. Abraham, Spectral hole burning and optically detected nuclear quadrupole resonance in flux-grown stoichiometric europium vanadate crystals, *Phys. Rev. B* **56**(1997), 7918–7929.

47. P.R. Hemmer, A.V. Turukhin, M.S. Shahriar, and J.A. Musser, Raman excited spin coherences in N-V diamond, *Optics Letters* **26**(2001), 361–363.

48. K. Holliday, M. Croci, E. Vauthey, and U.P. Wild, Spectral hole-burning and holography in an Y2SiO5Pr3+ crystal, *Phys. Rev. B* **47**(1993), 14741–14752.

49. J.P. Hornak, *http://www.cis.rit.edu/htbooks/nmr/inside.htm*.

50. F. Jelezko, and J. Wrachtrup, Quantum information processing in diamond , *quant-ph*/0510152.

51. F. Jelezko, T. Gaebel, I. Popa, M. Domhan, A. Gruber, and J. Wrachtrup, Observation of coherent oscillation of a single nuclear spin and realization of a two-qubit conditional quantum gate, *Phys. Rev. Lett.* **93**(2004), 130501.

52. J.A. Jones and M. Mosca, Implementation of a quantum algorithm on a nuclear magnetic resonance quantum computer, *J. Chem. Phys.* **109**(1998), 5, 1648–1653. Another short version can be found at *Nature* **393**(1998), 344–346.

53. J.A. Jones, Robust quantum information processing with techniques from liquid–state NMR, *Phil. Trans. Roy. Soc. Lond.* A **361**(2003), 1429 – 1440.

54. J.A. Jones, Robust Ising gates for practical quantum computation, *Phys. Rev. A* **67**(2003), 012317.

55. J.A. Jones, NMR quantum computation: a critical evaluation, *Fortschr. Phys.* **48**(2000), 909–924.

56. J.A. Jones, and E. Knill, Efficient refocusing of one–spin and two-spin interaction for NMR quantum computation, *J. of Magnetic Resonance* **141**(1999), 322 – 325.

57. B.E. Kane, A silicon-based nuclear spin quantum computer, *Nature* **393**(1998), 133–137.

58. N. Khaneja, R. Brockett, and S.J. Glaser, Time optimal control in spin system, *Phys. Rev. A* **63**(2001), 032308.

59. N. Khaneja, S.J. Glaser, and R. Brockett, Sub-Riemannian geometry and time optimal control of three spin systems: quantum gates and coherent transfer, *Phys. Rev. A* **65**(2002), 032301.

60. A.K. Khitrin, H. Sun, and B.M. Fung, Method of multifrequency excitation for creating pseudopure states for NMR quantum computing, *Phys. Rev. A* **63**(2001), 020301.

61. E. Knill, I. Chuang, and R. Laflamme, Effective pure states for bulk quantum computation, *Phys. Rev. A* **57**(1998), 3348.

62. E. Knill, R. Laflamme, R. Martinez, and C.H. Tseng, An algorithm benchmark for quantum information processing, *Nature* **404**(2000), 368–370.

63. E. Knill, R. Laflamme, R. Martinez, and C. Negrevergne, Benchmarking quantum computers: the five-qubit error correcting code, *Phys. Rev. Lett.* **86**(2001), 5811–5814.

64. E. Kupce, and R. Freeman, Close encounters between soft pulses, *J. of Magnetic Resonance Series A* **112**(1995), 261 – 264.

65. T.D. Ladd, D. Maryenko, Y. Yamamoto, E. Abe, and K.M. Itoh, Coherence time of decoupled nuclear spins in silicon, *Phys. Rev. B* **71**(2005), 014401.

66. T.D. Ladd, J.R. Goldman, F. Yamaguchi, and Y. Yamamoto, All-silicon quantum computer, *Phys. Rev. Lett.* **89**(2002), No. 1, 017901.

67. G.M. Leskowitz, N. Ghaderi, R.A. Olsen, and L.J. Mueller, Three-qubit nuclear magnetic resonance quantum information processing with a single-crystal solid, *J. Chem. Phys.* **119**(2003), 1643–1649.

68. D.W. Leung, I.L. Chuang, F. Yamaguchi, and Y. Yamamoto, Efficient implementation of coupled logic gates for quantum computation, *Phys. Rev. A* **61**(2000), 042310.

69. M.H. Levitt, Composite pulses, *Progress in Nuclear Magnetic Resonance Spectroscopy* **18**(1986), 61 – 122.

70. N. Linden, B. Herve, R.J. Carbajo and R. Freeman, Pulse sequences for NMR quantum computers: how to manipulate nuclear spins while freezing the motion of coupled neighbors, *Chem. Phys. Lett.* **305**(1999), 28–34.

71. N. Linden, H. Barjat, and R. Freeman, An implementation of the Deutsch-Jozsa algorithm on a three-qubit NMR quantum computer, *Chem. Phys. Lett.* **296**(1998), 61–67.

72. S.J. Lomonaco, Shor's Quantum Factoring Algorithm, *quant-ph*/0010034.

73. G. Long, H. Yan, Y. Li, C. Lu, J. Tao, and H. Chen et al., Experimental NMR realization of a generalized quantum search algorithm, *Physics Letters A* **286**(2001), 121 – 126.

74. J.J. Longdell, M.J. Sellars, and N.B. Manson, Hyperfine interaction in ground and excited states of praseodymium-doped yttrium orthosilicate, *Phys. Rev. B* **66**(2002), 035101.

75. J.J. Longdell and M.J. Sellars, Selecting ensembles for rare earth quantum computation, quant-ph/0310105, 2003.

76. J.J. Longdell, M.J. Sellars, and N.B. Manson, Demonstration of conditional quantum phase shift between ions in a solid, *Phys. Rev. Lett.* **93**(2004), 130503.

77. M.D. Lukin and P.R. Hemmer, Quantum Entanglement via Optical Control of Atom-Atom Interactions, *Phys. Rev. Lett.* **84**(2000), 2818–2821.

78. R.M. Macfarlane, High-resolution laser spectroscopy of rare-earth doped insulators: a personal perspective, *J. of Luminescence* **100**(2002), 1-4, 1–20.

79. M.L. Martin, and G.J. Martin, *Practical NMR Spectroscopy*, Heyden, London, U.K., 1980.

80. R. Laflamme, E. Knill, C. Negrevergne, R. Martinez, S. Sinha, and D.G. Cory, Introduction to NMR quantum information processing, in *Experimental Quantum Computation and Information, Proceeding of the International School of Physics "Enrico Fermi"*, edited by F. De Martini and C. Monroe, IOS Press, Amsterdam, Netherlands, 2002.

81. G.D. Mateescu and A. Valeriu, *2D NMR : Density Matrix and Product Operator Treatment*, PTR Prentice-Hall, New Jersey, 1993.

82. R. Marx, A.F. Fahmy, J.M. Myers, W. Bermel, and S.J. Glaser, Approaching five-bit NMR quantum computing, *Phys. Rev. A* **62**(2000), 012310.

83. M.A. Nielsen and I.L. Chuang, *Quantum Computation and Quantum Information*, Cambridge University Press, Cambridge, U.K., 2000.

84. M.A. Nielson and I.L. Chuang, Programmable quantum gate arrays, *Phys. Rev. Lett.* **79**(1997), 2, 321 − 323.

85. M.A. Nielson, E. Knill, and R. Laflamme, Complete quantum teleportation using NMR, *Nature* **396**(1995), 52–55.

86. J. Normand, *A Lie Group: Rotations in Quantum Mechanics*, North-Holland, New York, 1980.

87. S.L. Patt, Single- and multiple-frequency-shifted Laminar pulses, *J. of Magnetic Resonance* **96**(1992), 1, 94–102.

88. A.O. Pittenger, *An Introduction to Quantum Computing Algorithms*, Birkhauser, Boston, 2000.

89. C.P. Poole, and H.A. Farach, *Theory of Magnetic Resonance*, Wiley, New York, 1987.

90. I. Popa, T. Gaebel, M. Domhan, C. Wittmann, F. Jelezko, and J. Wrachtrup, Energy levels and decoherence properties of single electron and nuclear spins in a defect center in diamond, *quant-ph*/0409067, 2004

91. M.A. Pravia, Z. Chen, J. Yepez, and D.G. Cory, Towards a NMR implementation of a quantum lattice gas algorithm, *Computer Physics Communications* **146**(2002), Issue 3, 339–344.

92. G.J. Pryde GJ, M.J. Sellars, and N.B. Manson, Solid state coherent transient measurements using hard optical pulses, *Phys. Rev. Lett.* **84**(2000), 1152–1155.

93. R.L. Rivest, A. Shamir, and L. Adleman, A method of obtaining digital signature and public-key cryptosystems, *Communications of the ACM* **21**(1978), 120–126.

94. P.W. Shor, Polynomial-time algorithms for prime factorization and discrete logarithms on a quantum computer, *SIAM J. Comput* **26**(1997), 5, 1484–1509.

95. D. Simon, On the power of quantum computation, *Proceedings, 35th Annual Symposium on Foundations of Computer Science*(1994), IEEE Press, Los Alamitos, CA, 116-123.

96. S. Somaroo, C.H. Tseng, T.F. Havel, R. Laflamme, and D.G. Cory, Quantum simulation on a quantum computer, *Phys. Rev. Lett.* **82**(1999), 5381–5384.

97. O.W. Sorenson, Polorization transfer experiments in high-resolution NMR spectroscopy, *Progress of Nuclear Magnetic Resonance Spectroscopy* **21**(1989), Issue 6, 503–569.
98. M. Steffen, L.M.K. Vandersypen, and I.L. Chuang, Toward quantum computation: a five-qubit quantum processor, *IEEE Micro*, 24–34, 2001.
99. A. Szabo, Spin Dependence Of Optical Dephasing In Ruby - The Frozen Core, *Optics Letters* **8**(1983), 9, 486–487.
100. J.M. Taylor, H.A. Engel, W. Dur, A. Yacoby, C.M. Marcus, P. Zoller, and M.D. Lukin, Fault-tolerant architecture for quantum computation using electrically controlled semiconductor spins, *Nature Physics* **1**(2005), 3, 177–183.
101. A.M. Turing, On computable numbers, with an application to the Entscheidungs problem, *Proc. Lond. Math. Soc. 2* **42**(1936), 230.
102. G. Vahala, J. Yepez, and L. Vahala, Quantum lattice gas representation of some classical solitons, *Physics Letters A* **310**(2003), 187–196.
103. L. Vahala, G. Vahala, and J. Yepez, Lattice Boltzmann and quantum lattice gas representations of one-dimensional magnetohydrodynamic turbulence, *Physics Letters A* **306**(2003), 227–234.
104. L.M.K. Vandersypen, C.S. Yannoni, M.H. Sherwood, and I.L. Chuang, Realization of logically labeled effective pure states for bulk quantum computation, *Phys. Rev. Lett.* **83**(1999), 3085.
105. L.M.K. Vandersypen, M. Steffen, G. Breyta, C. Yannoni, R. Cleve, and I.L. Chuang, Experimental realization of an order-finding algorithm with an NMR quantum computer, *Phys. Rev. Lett.* **85**(2000), 5452.
106. L.M.K. Vandersypen, M. Steffen, M.H. Sherwood, C. Yannoni, G. Breyta, and I.L. Chuang, Implementation of a three-quantum-bit search algorithm, *Applied Physics Letters* **76**(2000), 5, 646–648.
107. L.M.K. Vandersypen, and I.L. Chuang, NMR techniques for quantum control and computation, *Reviews of Modern Physics* **76**(2004), 4, 1037–1069.
108. E. van Oort, N.B. Manson, and M. Glasbeek, Optically detected spin coherence of the diamond N-V center in its triplet ground-state , *J. of Physics C-Solid State Physics* **21**(1988), 4385–4391.
109. L.M.K. Vandersypen, M. Steffen, G. Breyta, et al., Experimental realization of Shor's quantum factoring algorithm using nuclear magnetic resonance. *Nature* **414**(2001), 883–887.
110. V. Vedral, A. Barenco, and A. Ekert, Quantum network for elementary arithmetic operations, *Phys. Rev. A* **54**(1996), 147–153.
111. C. Wei, and N.B. Manson, Observation of electromagnetically induced transparency within an electron spin resonance transition, *J. of Optics B-Quantum and Semiclassical Optics* **1**(1999), 464–468.
112. Y.S. Weinstein, M.A. Pravia, E.M. Fortunato, S. Lloyd, and D.G. Cory, Implementation of the quantum Fourier transform, *Phys. Rev. Lett.* **86**(2001), 1889–1891.
113. Wikipedia, *http://en.wikipedia.org/wiki/Nuclear_magnetic_resonance.*
114. F. Yamaguchi, and Y. Yamamoto, Crystal lattice quantum computer, *Microelectronic Engineering*, **47**(1999), 273–275.
115. C. Yannoni, M.H. Sherwood, D.C. Miller, I.L. Chuang, L.M.K. Vandersypen, and M.G. Kubines, Nuclear magnetic resonance quantum computing using liquid crystal solvents, *Applied Physics Letter* **75**(1999), No. 22, 3563–3562.
116. A. Yao, Quantum circuit complexity, *Proc. of the 34th Ann. IEEE Symp. on Foundations of Computer Science*(1993), 352-361.

117. J. Yepez, Quantum lattice-gas model for the diffusion equation, *International Journal of Modern Physics C* **12**(2001), 9, 1285–1303.

118. J. Yepez, Type-II quantum computers, *International Journal of Modern Physics C* **12**(2001), 9, 1273–1284.

119. J. Yepez, and B. Boghosian, An efficient and accurate quantum lattice-gas model for the many-body Schrödinger wave equation, *Computer Physics Communications* **146**(2002), Issue 3, 280–294.

120. J. Zhang, Z. Lu, L. Shan, and Z. Deng, Synthesizing NMR analogs of Einstein-Podolsky-Rosen state using the generalized Grover's algorithm, *Phys. Rev. A* **66** (2002), 044308.